



Det här verket är upphovrättskyddat enligt *Lagen (1960:729) om upphovsrätt till litterära och konstnärliga verk*. Det har digitaliserats med stöd av Kap. 1, 16 § första stycket p 1, för forskningsändamål, och får inte spridas vidare till allmänheten utan upphovsrättsinnehavarens medgivande.

Alla tryckta texter är OCR-tolkade till maskinläsbar text. Det betyder att du kan söka och kopiera texten från dokumentet. Vissa äldre dokument med dåligt tryck kan vara svåra att OCR-tolka korrekt vilket medför att den OCR-tolkade texten kan innehålla fel och därför bör man visuellt jämföra med verkets bilder för att avgöra vad som är riktigt.

This work is protected by Swedish Copyright Law (*Lagen (1960:729) om upphovsrätt till litterära och konstnärliga verk*). It has been digitized with support of Kap. 1, 16 § första stycket p 1, for scientific purpose, and may no be disseminated to the public without consent of the copyright holder.

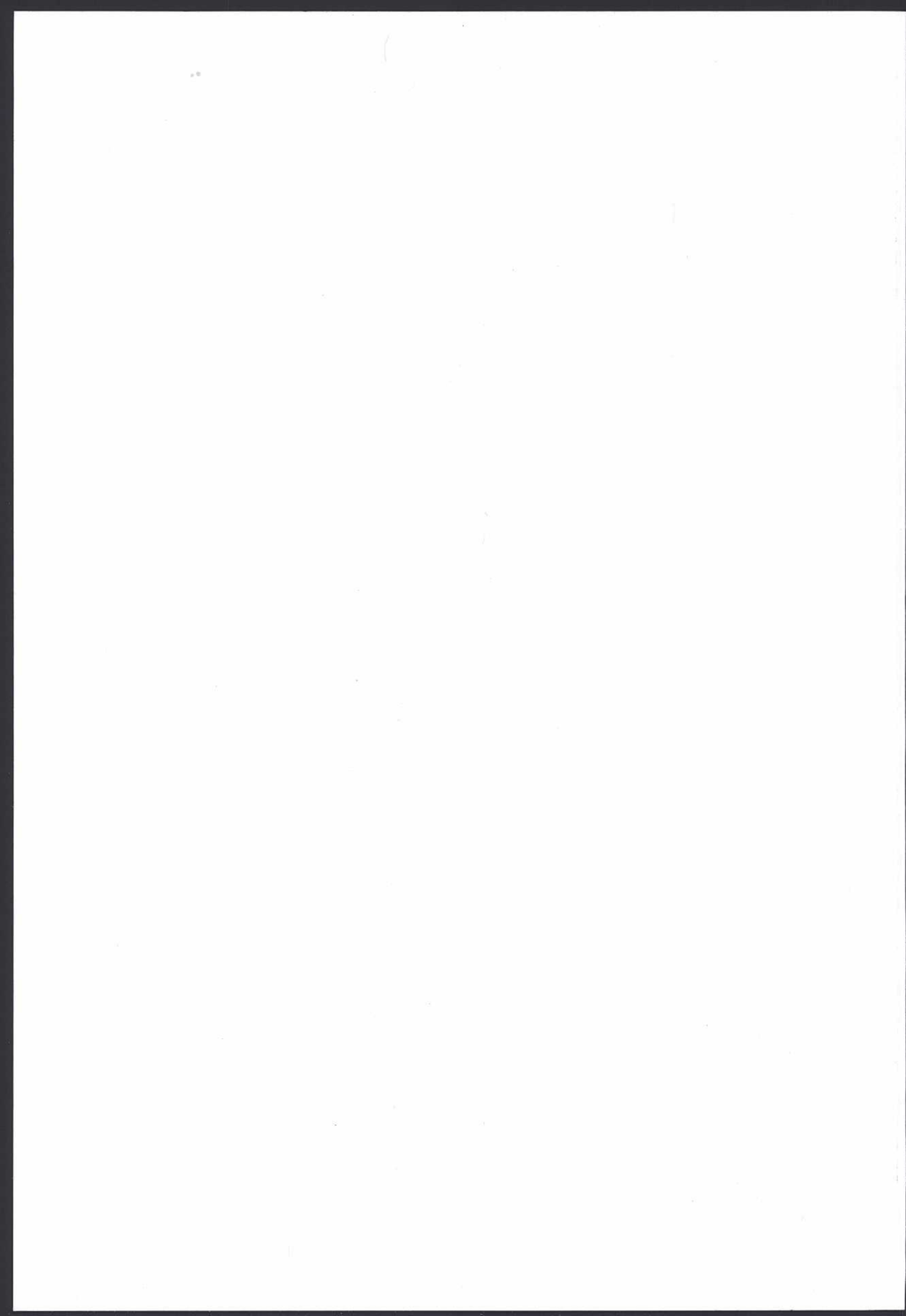
All printed texts have been OCR-processed and converted to machine readable text. This means that you can search and copy text from the document. Some early printed books are hard to OCR-process correctly and the text may contain errors, so one should always visually compare it with the images to determine what is correct.



# Modelling and Data Analysis, Tools for Understanding of Chemical Processes in Troposphere

JANA MOLDANOVÁ  
Department of Chemistry  
Göteborg University





Göteborgs Universitet

Modelling and Data Analysis,  
Tools for Understanding of Chemical Processes in  
Troposphere

Jana Moldanová



Akademisk avhandling

för avläggande av filosofie doktorsexamen i Miljövetenskap med inriktning mot oorganisk kemi.

Med tillstånd av sektionen för Miljövetenskap vid Göteborgs Universitet

försvaras avhandlingen offentligt onsdagen den 31 maj 2000 kl 10<sup>15</sup>

i sal KS 101, Kemihuset, Chalmers.

Fakultetsopponent är Dr. R. G. Derwent, Meteorological Office, Bracknell, UK.

Institutionen för Kemi  
Oorganisk Kemi  
412 96 Göteborg



Modelling and Data Analysis, Tools for Understanding  
of Chemical Processes in Troposphere

ISBN 91-628-4220-X

Published in Göteborg, Sweden, May 2000

Printed in Chalmers Reproservice

# Abstract

Human activities significantly altered the atmosphere of planet Earth during the past century. Each second, tons of man-made nitrogen oxides ( $\text{NO}_x$ ) and volatile organic compounds (VOC) are emitted to the air around the globe. These species can react in the gas phase and form ozone and other secondary pollutants. They can also be transferred to the condensed phase, or may be removed by deposition at the Earth surface. The man-made emissions can also interact with naturally emitted gases and particles. Since the natural emissions are often larger than the man made ones, they are of great interest to atmospheric science. This thesis investigates several aspects of formation of secondary pollutants and removal of VOC by using numerical models and by analysing environmental measurements and experimental data.

Concentrations of 9 hydrocarbon species and ozone at background station Rörvik, situated south of Göteborg, Sweden, measured continuously during a two-year period, were analysed. The statistical analysis showed groups of individual species with high internal correlation and also a distinct seasonal variation of some species. Variation with the origin of the air mass showed, that the major part of hydrocarbons and ozone at the Swedish West Coast is transported from central and Western Europe or from the UK. The measured concentrations were simulated by a Lagrangean trajectory photochemical model. The sensitivity analysis performed illustrated well the importance of some processes described by the model.

Sea-salt is emitted in huge amounts to the atmosphere in the form of solution droplets. During the time the droplets stay suspended in the troposphere, they can release active halogen species to the troposphere. Such compounds may form atomic halogens, which can initialise oxidation of VOC and hence increase the oxidation capacity of the troposphere. A numerical model CCDSSP was developed to investigate the halogen release from the sea-salt particles and its effect on VOC degradation and photooxidant formation. The model includes a detailed description of both gas and aqueous phase chemistry with focus on the chemistry of chlorine and bromine. Mechanisms of halogen release and the effect on the coastal air and on acid deposition are discussed. The model results are compared with available measurements of active halogen species and of the deposited sea-salt.

Monoterpenes are biogenic VOC, emitted in large quantities from vegetation. A common phenomenon observed in terpene oxidation experiments is formation of particulate matter. Particle size distribution and particle number concentration data from experiments with oxidation of four monoterpene species were analysed and equilibrium vapour pressures of the main condensing products were estimated. The nucleation process was parametrised, using the measured data. A model simulating gas-to-particle conversion was developed. Processes affecting the measured final particle size distributions and implications for the environmental modelling are discussed.

Keywords: numerical model; data analysis; tropospheric chemistry; VOC; NMHC; halogens; Cl-atom; Br-atom; sea-salt; gas to particle conversion; BVOC; monoterpenes;

Published in Göteborg, May 2000, ISBN 91-628-4220-X  
49 pages + 5 appended papers

## Enclosed Papers

This thesis is based on the work presented in the following papers. In the text, they will be referred to by their roman numerals.

- I. The influence of the origin, season and time of the day on the distribution of individual NMHC measured at Rörvik, Sweden. A. Lindskog and J. Moldanová, *Atmos. Environ.*, **15**, 2383-2398, (1994).
- II. Comparison of Simulated and Measured Concentrations of Ozone, PAN and Organic Species - Influence of Chemical Activity and Emission Pattern. Y. Andersson-Sköld, J. Moldanová and A. Lindskog, *The Proceedings of EUROTRAC Symposium '92*, ed. Borell et al, SPB Academic Publishing, Haag, pp. 433-436, (1992).
- III. Description of the chemistry of chlorine species for use in a regional tropospheric model. J. Moldanová and E. Ljungström, *Proceedings of the 10<sup>th</sup> World Clean Air Congress*, The Finnish Air Pollution Prevention Society, Espoo, May 28-June 2, p. 319, (1995).
- IV. Sea salt aerosol chemistry in coastal areas. A model study, J. Moldanová, E. Ljungström, Submitted to *J. Geophys. Res.*
- V. Modelling of particle formation from NO<sub>3</sub> oxidation of selected monoterpenes, J. Moldanová and E. Ljungström, *J. Aerosol Sci.*, in print.

## Table of contents

1. Introduction .....	1
2. Gas phase reactions in troposphere .....	5
2.1. Basic day-time processes .....	5
2.2. Night-time chemistry .....	7
2.3. Chemistry of halogen species .....	8
3. Reactions in aqueous particles .....	11
3.1. Chemistry of sea-salt particles .....	12
4. Photolysis rates .....	17
5. Transport processes .....	19
5.1. Exchange of mass at the gas-particle interface .....	19
5.2. Limitation of reaction rates by aqueous phase diffusion .....	20
5.3. Fluxes and concentrations of sea-salt particles .....	21
5.4. Deposition .....	22
6. Mathematical description .....	25
6.1. Analysis of measured concentrations .....	25
6.2. Numerical models .....	26
7. Results and discussion .....	29
7.1. Concentrations of NMHC and ozone .....	29
7.2. Halogen chemistry in the troposphere .....	32
7.3. Effects of sea-salt particles on the troposphere in coastal areas .....	34
7.4. Formation of particles from oxidation products of monoterpenes .....	37
8. Conclusions .....	41
References .....	45



# 1. Introduction

Successful investigations of atmospheric composition go back to the eighteenth century, when the major constituents, nitrogen and oxygen were identified. Since then, many other components, including water vapour, carbon dioxide, and the noble gases were discovered. In fact, if proper analysis techniques are applied, hundreds of trace gases may be found in polluted air. A number of them, though present in concentrations lower than 1 part per million (ppm,  $\mu\text{mole/mole}$ ), play an important role in processes affecting air quality, solar radiation at the Earth's surface, and climate. Traces conserved in glacial ice and in sediments, together with long term atmospheric monitoring, reveal that human activities have significantly altered the composition of the atmosphere during the passed century. A steadily increasing concentration of carbon dioxide ( $\text{CO}_2$ ), increasing the greenhouse effect, and the depletion of stratospheric ozone caused by the release of CFC-gases are examples of the global influence of human activities on Earth's atmosphere. Also phenomena developed on a limited scale, both in time and space, such as London and Los Angeles-type smogs, have effects of a large-scale character. Such effects are e.g. acid rain and enhanced concentrations of tropospheric ozone.

Gaining knowledge about a chemical process in the atmosphere usually proceeds in several steps. Environmental monitoring identifies the main species involved and the available chemical and physical knowledge is applied. Laboratory experiments are often needed to complement the knowledge about the processes involved. A simple model involving only basic reactions or steady-state approximations is usually set up in order to understand all relations between the species and processes. The steady-state approximation is often unrealistic when considering the real atmosphere, especially when regarding the major oxidising species, i. e. hydroxyl radicals ( $\text{OH}$ ), ozone, and nitrate radicals ( $\text{NO}_3$ ), which closely connect the chemical reactions. If the role of these species needs to be described explicitly, rather extended chemical schemes have to be devised and the simple model becomes more complicated. The results of such model calculations are still rather limited in application on measured concentrations since the description of transport is very simplified or absent. The results can often point out missing parts and may serve as a base for a more detailed transport model.

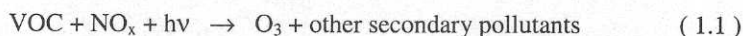
Meteorology and atmospheric chemistry in general deal with the lower atmosphere, which extends to an altitude of approximately 50 km. Based on the vertical temperature profile, two layers can be distinguished within this region. The lower part, characterised by a linear temperature decrease ( $9.7 \text{ K km}^{-1}$  for the dry air) is known as the troposphere. The word originates from the Greek *tropos*, turning, pointing at the important property of the troposphere, turbulence and mixing. The height of troposphere ranges from 18 km above the equator to less than 10 km above the poles. The first kilometre or so above the ground is called the planetary boundary layer, sometimes also the mixing layer, while the upper part of the region is called the free troposphere. The upper layer, extending from about 10 to 50 km is called the stratosphere. The temperature is low and stable up to the 20 km altitude. Then it



starts to increase up to 50 km, where it reaches a temperature similar to that at the Earth's surface. The name, originating from the Latin word *stratum*, layer, reflects the temperature stability in its lower part, discovered at the turn of the 20<sup>th</sup> century. Stratosphere, in difference from troposphere, is a stable layer with limited vertical transport. The work described in this thesis is concerned with the troposphere.

A mathematical model, describing the real troposphere must synthesise knowledge from chemical kinetics, photochemistry, atmospheric physics, meteorology, and environmental monitoring. A numerical model that would simulate all atmospheric processes explicitly and in detail is not realistic. Besides the fact that our understanding is far from complete, such a model would be too demanding on input data and computer capacity. Simplifications, generalisations, and compromises are therefore necessary. There are two principally different types of numerical models used in atmospheric chemistry. While the Eulerian model describes transport of chemical components on a two or three-dimensional grid with fixed coordinates, the Lagrangean model follows one air mass along its trajectory. Eulerian models are better suited to study three-dimensional transport problems, but are often demanding in terms of computer capacity. The advantage of Lagrangean models is the direct source-receiver relationship and the possibility of following the chemical development of one air mass.

An alteration of atmospheric composition brings about an alteration of its oxidising capacity, i.e. the capacity to deal with various pollutants. Ozone formation from nitrogen oxides (NO<sub>x</sub>) and Volatile Organic Compounds (VOC) is very closely coupled to this property of the atmosphere. The increase of ozone concentration in the troposphere (Bojkov, 1986, Staehelin and Schmid, 1991) is believed to be caused by *in situ* formation in the background air (Crutzen, 1983, Austin and Follows, 1991). The mechanism driving the ozone photochemistry in the lower troposphere is coupled with the NO<sub>x</sub>-cycle, oxidation of VOC, and with formation of other secondary pollutants. Finlayson-Pitts and Pitts (2000) describes the system in a general form:



A variety of VOC, emitted both naturally and from human activities, is present in the troposphere. They are mainly removed by oxidation, initiated by free radicals present in very low concentrations. A free radical is an atom or molecule with at least one unpaired electron that makes the species highly reactive. The lifetime of organic species in the troposphere range from several years for methane to less than one hour for some conjugated unsaturated hydrocarbons. While the long-lived species are believed to be responsible for the increase of ozone concentration in the free troposphere, more reactive species dominate the ozone production in the polluted boundary layer. If atomic halogen species are present, then the oxidation rate of some VOC increases. It was peculiarities in concentration ratios for some hydrocarbons that were transported over the ocean, that started the discussion about the importance of halogens in tropospheric chemistry (Finlayson-Pitts, 1993, Jobson *et al.*, 1994).

To increase the knowledge about formation of ozone and other photochemical oxidants, a large number of campaigns and also continuous measurements have been conducted and are in progress around the world. Concentration levels of NO<sub>x</sub>, ozone, Peroxy-Acetyl Nitrate

(PAN), and some VOC are nowadays reasonably well known in many regions. One of the major joint European projects on transport and transformation of pollutants was EUROTRAC (European Experiment on Transport and Transformation of Environmentally Relevant TRACe Constituents in the Troposphere over Europe). The sub-project TOR (Tropospheric Ozone Research) was focused on the distribution and trends in concentrations and on the transport of ozone and its precursors. Within the TOR project, a network of background monitoring stations covering Europe was established. One of the TOR monitoring stations was situated on the Swedish West Coast at Rörvik, south of Göteborg. It was established as a TOR station in 1989 and individual NMHC, O<sub>3</sub>, SO<sub>2</sub>, NO<sub>2</sub>, sulphate, nitrate and ammonium were measured at Rörvik within the TOR and EMEP-network (European Monitoring and Evaluation Programme). These data were used as the basic information for photo oxidant modelling, giving concentration levels both for initial concentrations and for model validation.

About 7% of the 6000 Tg Cl in the sea-salt-aerosol generated annually over the sea are deposited on land (Graedel and Keene, 1995). During the time the seawater droplets stay suspended, they may contribute to the chemistry of both the marine and continental troposphere. The most well documented process is the uptake of strong acids or their precursors with a subsequent release of HCl to the gas-phase. (Junge, 1957, Keene *et al.*, 1990, Laux *et al.*, 1994). Several other mechanisms have been proposed for the release of halogens (Finlayson-Pitts *et al.*, 1989, Behnke *et al.*, 1997, Laux *et al.*, 1994, Behnke and Zetzsch, 1989, Mozurkewich, 1995, Vogt *et al.*, 1996). The role of Cl and Br radicals in the tropospheric ozone cycle is more complex than just by initiating VOC oxidation. Both react with ozone, creating a catalytic X – XO cycle. In clean troposphere, the cycle is to a large extent closed by reactions that do not reform O<sub>3</sub> and therefore lead to a reduction of the O<sub>3</sub> concentration (Barrie *et al.*, 1988, LeBras *et al.*, 1995).

To be able to quantify the effect of anthropogenic emissions on atmospheric composition, also natural emissions have to be considered. Intense research on Biogenic Volatile Organic Compounds (BVOC) has sprung from the awareness of the enormous quantities of such compounds that are emitted to the atmosphere (Arnts and Meeks, 1981, Lamb *et al.*, 1987, Monson *et al.*, 1992, Guenther *et al.*, 1995, Simpson *et al.*, 1999). A large fraction of the emitted BVOC is made up by monoterpenes (general formula C<sub>10</sub>H<sub>16</sub>) (Guenther *et al.*, 1995). Monoterpenes are very reactive with hydroxyl and nitrate radicals and also with ozone (Atkinson, 1997). One common feature of laboratory investigations of monoterpene oxidation is the formation of particulate matter. Since particles influence important atmospheric processes such as light scattering and cloud formation (Andreae and Crutzen, 1997), new particle formation from natural sources is of great importance in describing e.g. the planet Earth's energy balance.

Several aspects of atmospheric chemistry have been addressed in this thesis. In Paper I, background concentrations of individual hydrocarbons and of ozone, measured at Rörvik were analysed and the data variability interpreted in terms of photochemical and transport processes affecting tropospheric chemistry in the northern part of Europe. Data from the same monitoring station were compared with back-trajectory model simulations in Paper II and the effect of processes described by the model on VOC and ozone concentrations were investi-



gated. In Paper III, the gas-phase tropospheric chemistry and the diurnal variability of chlorine species were investigated. This study was done in preparation for Paper IV, where a model called "Coastal Chemistry and Deposition of Sea-Salt Particles" (CCDSSP) was developed. Paper V concerns the formation of particles from terpenes. Data from experiments performed in the large EUPHORE photochemical reactor (Hallquist *et al.*, 1999) were analysed and vapour pressures and nucleation rates were estimated. Within this study, a model simulating the nucleation and gas-to-particle conversion of terpene oxidation products was developed in order to gain an understanding of the observed size distributions.

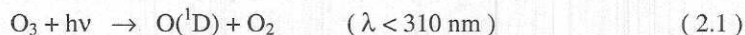
## 2. Gas phase reactions in troposphere

The gas phase processes described in this section are fundamental for models and interpretations presented in this thesis. Papers I-IV are concerned with the daytime photochemistry, presented in section 2.1. All papers include the nighttime chemistry with the  $\text{NO}_3$  radical initiated oxidation of VOC, described in section 2.2. Papers II, III and IV also utilise the halogen chemistry, described in section 2.3.

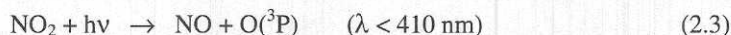
### 2.1. Basic day-time processes

Tropospheric chemistry is to a large extent driven by solar radiation. The major constituents of the atmosphere do not become photolysed at ground level since the wavelengths necessary for the photodissociation were already absorbed at higher levels in the atmosphere. Some of the trace gases emitted at the Earth's surface, or transported from higher altitudes can, however, photodissociate and form radical species that may start oxidation chain reactions.

The most important oxidising species in the troposphere is the hydroxyl radical (OH). The main source of hydroxyl radicals is the reaction of  $\text{O}(^1\text{D})$  (excited) atoms with water vapour,

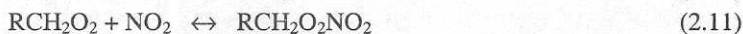
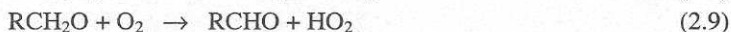
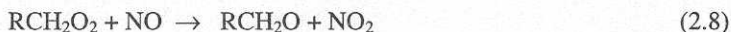


Ozone is a trace gas present in the troposphere in low concentrations (tens to hundreds ppb, nmole/mole). Its origin is either by *in situ* formation from oxides of nitrogen and hydrocarbons or by transport from the stratosphere. In a sun-irradiated troposphere containing  $\text{NO}_2$ , but no peroxy radicals, a steady state ozone concentration would be established by reactions (2.3) through (2.5).

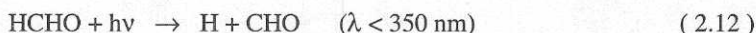


M is any molecule that could absorb energy. During the photochemical breakdown of hydrocarbons, organic peroxy radicals ( $\text{RCH}_2\text{O}_2$ ) and hydroperoxy radicals ( $\text{HO}_2$ ) are formed. The formation is initiated by the attack of e.g. OH radicals on an alkane molecule according to reaction (2.6). A peroxy-radical is then formed by an addition of molecular oxygen to the primary alkyl radical according to (2.7). These peroxy radicals compete with  $\text{O}_3$  for the NO to  $\text{NO}_2$  conversion via reaction (2.5) by opening reaction channels (2.8) and (2.10). One molecule of  $\text{O}_3$  is consumed in reaction (2.5), but there is no  $\text{O}_3$  consumption in

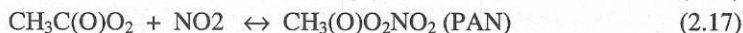
NO to NO<sub>2</sub> conversion by peroxy radicals (reactions 2.8 and 2.10). Since O<sub>3</sub> is formed during the photolysis of NO<sub>2</sub>, the net effect of (2.8) and (2.10) is to cause a net O<sub>3</sub> production. The peculiar role of O<sub>3</sub> in the atmosphere is illustrated by the fact that on the one hand O<sub>3</sub> is needed to produce OH-radicals necessary to maintain the atmospheric oxidation capacity, and on the other hand is a result of VOC oxidation in the presence of NO<sub>x</sub>. Reaction (2.6) through (2.10) give an example of the first part of the photochemical breakdown of a hydrocarbon molecule. It can be noted that the OH-radical consumed in (2.6) is re-formed in (2.10). Typical lifetimes for reaction of the OH-radical with some VOC are presented in Table 1. Organic peroxy radicals formed in reaction (2.7) can also react with NO<sub>2</sub> to form organic peroxy nitrates (2.11). Organic peroxy nitrates undergo thermal decomposition, which is strongly temperature dependent (DeMore *et al.*, 1997). Consequently, winter conditions with low temperatures favour the accumulation of organic peroxy nitrates.



In the background air a smaller source of OH radicals is the photolysis of aldehydes. Aldehydes are stable organic species, which are emitted both from anthropogenic and natural sources and produced during the photochemical breakdown of hydrocarbons (reaction 2.9). The photolysis of formaldehyde (2.12) and subsequent reactions (2.13) and (2.14) is an example of this process. Reactions (2.13) and (2.14) are followed by reaction (2.10) and two OH radicals are formed.



A peroxy-acetyl radical is formed by OH attack on acetaldehyde (2.15), followed by O<sub>2</sub> addition (2.16). This is the precursor for PAN, an important secondary pollutant present in photochemical smog, formed through (2.17). PAN and other peroxy nitrates can act as a reservoir for nitrogen oxides and also of OH radicals, as HO<sub>2</sub> is formed by (2.9) and by a corresponding reaction sequence of the peroxy-acetyl radical when the equilibrium (2.11) or (2.17) shifts and the peroxy- and peroxy-acetyl nitrates decompose thermally.



The terminating steps for the OH-carried chain are reactions with NO<sub>2</sub>, HO<sub>2</sub> or self-reaction between two HO<sub>2</sub> radicals (2.18 through 2.20). Both nitric acid, formed by reaction (2.18), and hydrogen peroxide, formed by reaction (2.19), is removed from the air by depo-

sition. In an atmospheric environment rich in oxides of nitrogen, such as Europe, reaction (2.18) is the most important sink of OH radicals (Platt *et al.*, 1988). Reaction (2.19) and (2.20) may gain importance in very clean areas such as Antarctica or over remote oceans.

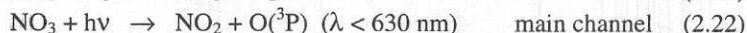


Equation (2.1) implies that the rate of VOC removal through the OH cycle is strongly dependent on solar radiation intensity and on air humidity. The oxidising capacity of the air around equatorial latitudes with high humidity is therefore higher than that of the relatively drier air of mid latitudes. Number of measurements of OH radical concentrations is available for the northern mid-latitudes. The summer noon concentrations at cloud-free sky range between 3 and  $15 \times 10^6$  molec.  $\text{cm}^{-3}$ , the higher value being coupled with pollution episodes (Perner *et al.*, 1987, Mount *et al.*, 1997, Holland *et al.*, 1998).

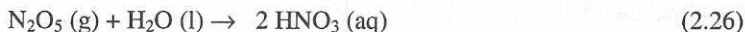
Oxidation of unsaturated VOC by the OH radical is fast and proceeds *via* addition to the double bond. Final products are often multi-functional species with hydroxyl, carbonyl and nitrate groups. Unsaturated hydrocarbon oxidation can also be initiated by reaction with ozone. Ozonolysis reaction mechanisms are quite complex and in many cases not fully understood. Ozonolysis of alkenes may act as a small OH source (Finlayson-Pitts and Pitts, 2000). Even though rate constants for  $\text{O}_3$ -initiated reactions are smaller than those of OH, the lifetimes of unsaturated VOC with respect to these reactions are of the same order of magnitude since the ozone concentration is roughly  $10^6$  times higher than that of OH. Thus, the removal of unsaturated VOC species by ozone can become quite important under specific conditions (Finlayson-Pitts and Pitts, 2000). This is well illustrated in Table 1.

## 2.2. Night-time chemistry

Another radical that can initiate breakdown of some VOC, is the nitrate radical ( $\text{NO}_3$ ). The  $\text{NO}_3$  source is the reaction of  $\text{NO}_2$  with ozone (2.21). The  $\text{NO}_3$  is rapidly photolysed during daytime (2.22 and 2.23). Therefore, accumulation is possible only during night, when the main loss reactions are with NO (2.24) and with alkenes (Finlayson-Pitts and Pitts, 2000). Dinitrogen pentoxide ( $\text{N}_2\text{O}_5$ ) plays an important role in the  $\text{NO}_3$  chemistry as it acts as a temporary reservoir of  $\text{NO}_3$  through the equilibrium reaction with  $\text{NO}_2$ . Equilibrium (2.25) controls the  $\text{NO}_3$  concentration at night. The removal of  $\text{N}_2\text{O}_5$  is an important loss process for  $\text{NO}_x$  and, at the same time, a sink for  $\text{NO}_3$  radicals.  $\text{N}_2\text{O}_5$  reacts heterogeneously with liquid water according to (2.26) and is subsequently washed out from the atmosphere.







Heintz *et al.* (1996) measured  $\text{NO}_3$  concentrations at a rural site in North Germany during a 14 months period. They found the highest  $\text{NO}_3$  concentrations in spring, reaching values of nearly  $2.5 \times 10^9$  molec.  $\text{cm}^{-3}$  in an episode. During summer, the peak values varied between  $1.5$  and  $2.5 \times 10^8$ . The winter  $\text{NO}_3$  peak concentrations were close to the detection limit of  $5 \times 10^7$  molec.  $\text{cm}^{-3}$ . According to Heintz *et al.* (1996)  $\text{NO}_3$  concentrations usually ranged between  $2.5 \times 10^8$  and  $5 \times 10^9$  molec.  $\text{cm}^{-3}$ , the lower values being typical for clean or slightly polluted air and the higher values for polluted air.

The  $\text{NO}_3$  radical starts the oxidation of unsaturated VOC by adding to one of the carbon atoms of a double bond. The presence of conjugated double bonds and alkyl substituents cause a dramatic increase in reaction rate (Noda *et al.*, 2000). Di-carboxylic acids have recently been identified as low-yield products. These acids have extremely low vapour pressures and could possibly lead to the formation of condensed matter.

The reaction between  $\text{NO}_3$  and saturated VOC proceeds *via* H atom abstraction forming nitric acid ( $\text{HNO}_3$ ) and a peroxy radical. These reactions are quite slow, compared to those with OH, but occasionally they can become important during the dark periods. Lifetimes with respect to  $\text{NO}_3$  reaction of some C2-C5 hydrocarbons are presented in Table 1.

### 2.3. Chemistry of halogen species

Seawater contains halogens in the form of chloride (97 mole % of anions) and bromide (0.3 %). Huge amounts of seawater are transferred to the atmosphere from the sea surface as small droplets. Even if only a small part of the halogens would be released from the droplets, the importance of halogen species would have to be considered. Halogens may be released from the droplets in the form of hydrochloric acid (HCl), molecular halogens ( $\text{Cl}_2$  or  $\text{Br}_2$ ), bromine-chloride (BrCl), hypohalogenous acids (HOCl or HOBr), nitrosyl halides (NOCl or NOBr), or nitryl halides ( $\text{ClNO}_2$  or  $\text{BrNO}_2$ ). These species may form atomic halogens either by reacting with OH (2.28), or by photolysis, as illustrated by reaction (2.29) through (2.32). In the following, X will be used to designate Cl or Br.



Atomic Cl and Br can react with ozone, forming a halogen monoxide radical (reaction 2.33). This reaction is one part of a catalytic reaction cycle, with halogen X as a catalyst, which is completed by one of the reactions 2.34 through 2.36.





(Followed by 2.30 gives X + OH)



In contrast to ClO, BrO is easily photolysed, yielding Br and an O(<sup>3</sup>P) atom. The tropospheric catalytic halogen cycles may have an ozone depleting effect, which is especially pronounced in a clean environment. When the photochemical system is limited by the availability of NO<sub>x</sub>, then reactions (2.35) and (2.36) are not producing ozone and the net result is the removal of one ozone molecule. When the environment is rich in NO<sub>x</sub> and limited in peroxy radicals, the ozone forming reaction (2.34) gains in importance and (2.36) also yields ozone when followed by reaction with NO (2.10). The effect of the catalytic cycle on ozone concentration is thus reduced. The BrO photolysis also yields ozone and reduces the ozone depleting effect of the Br-BrO cycle.

When NO<sub>2</sub> is present in atmosphere, chlorine monoxide equilibrates with chlorine nitrate (ClONO<sub>2</sub>) and a similar equilibrium is also set-up for bromine. The XONO<sub>2</sub> species are more important in winter, as their equilibria shifts towards ClONO<sub>2</sub> and BrONO<sub>2</sub> at lower temperatures. XNO<sub>2</sub>, the photolysis of which is described by (2.32), can also be formed in the gas phase by reaction between atomic halogen and NO<sub>2</sub>. The last of the reactive halogen species studied in Papers III and IV is the nitrosyl chloride, ClNO, which is formed by the reaction of Cl with NO and which is photolysed by sunlight according to (2.31).

Chlorine attack on saturated hydrocarbons starts with an H atom abstraction and the formation of HCl. These reactions are fast. The reaction of bromine atoms with alkanes is extremely slow. The chlorine and bromine initiated degradation of unsaturated hydrocarbons leads to the formation of halogenated aldehydes and ketones during the reaction chain, finally forming, among other products, CHClO and CHBrO (Niki *et al.*, 1980, Lee and Rowland, 1977, Niki *et al.*, 1987).

**Table 1.** Lifetimes of some VOC with respect to the reactions with OH, NO<sub>3</sub>, Cl and Br radicals and with ozone. The figures in bold style are lifetimes in days, otherwise lifetimes in hours are given. Concentrations of the radical species used for the lifetime calculation are (in molec. m<sup>-3</sup>) 2.6×10<sup>6</sup> OH (Holland et al., 1998), 2.5×10<sup>8</sup> NO<sub>3</sub> (Heintz et al., 1996), 5×10<sup>3</sup> Cl, 2×10<sup>5</sup> Br (Paper IV), 5.1×10<sup>11</sup> O<sub>3</sub> (Paper I).

species	$\tau$ (days, hr)				
	OH	NO <sub>3</sub>	Cl	Br	O <sub>3</sub>
CO	<b>21</b>				
methane	<b>907</b>				
ethane	511		<b>41</b>		
propane	101	<b>2104</b>	<b>17</b>		
n-butane	44	<b>1522</b>	<b>12</b>		
i-butane	327	<b>543</b>	<b>17</b>		
n-pentane	284	<b>572</b>	<b>9</b>		
i-pentane	27	<b>365</b>	<b>9</b>		
ethene	13	<b>320</b>	<b>21</b>	<b>445</b>	<b>18</b>
acetylene	141	<b>926</b>	<b>38</b>		
parafine	134		463		
olefin	4	146	228	514	60
$\alpha$ -pinene	2.0	0.2	-	-	6
$\beta$ -pinene	1.4	0.4	-	-	36
$\Delta$ 3-carene	1.2	0.1	113	-	15
limonene	0.6	0.1	-	-	3

### 3. Reactions in aqueous particles

Many gases emitted at the Earth's surface are water soluble, such as SO<sub>2</sub>, NH<sub>3</sub>, some organic compounds, and so are some species produced in the troposphere, such as HNO<sub>3</sub> and HCl. Radical species, e.g. OH, HO<sub>2</sub>, and NO<sub>3</sub> may also dissolve into the droplet and start oxidation reactions. Henry's law (3.1) describes equilibrium between species A, present at a partial pressure p<sub>A</sub> in the gas phase, and in a concentration [A] in the aqueous phase.

$$[A] = p_A \times H_A, \quad (3.1)$$

H<sub>A</sub> is the Henry's law constant (mol atm<sup>-1</sup>). The equilibrium equations and Henry's law constants of species dissolving in the aqueous phase employed in the CCDSSP model are presented in Table 9, Paper V.

Nitric, sulphuric, hydrochloric and hydrobromic acids (HNO<sub>3</sub>, H<sub>2</sub>SO<sub>4</sub>, HCl and HBr) are strong acids that are highly soluble in water. The effective Henry's law constant, describing the total amount of HNO<sub>3</sub> in both undissociated and dissociated form in the liquid, has the form

$$H_{HNO_3}^* = H_{HNO_3} \left( 1 + \frac{K_{N1}}{[H^+]} \right) \quad (3.2)$$

The dissociation constant K<sub>N1</sub> for HNO<sub>3</sub> is 15.4 M at 298K and is so high, that K<sub>N1</sub>/[H<sup>+</sup>] >> 1 and the effective Henry's law constant can be approximated by H<sub>HNO<sub>3</sub></sub>K<sub>N1</sub>/[H<sup>+</sup>] = 2.42×10<sup>6</sup>/[H<sup>+</sup>] and the concentration of undissociated HNO<sub>3</sub> can be neglected. Hydrochloric and hydrobromic acids with dissociation constants K<sub>HCl</sub> = 1.74×10<sup>6</sup> and K<sub>HBr</sub> = 1×10<sup>9</sup> (Seinfeld and Pandis, 1998) can also be assumed to be fully dissociated. The first dissociation constant of H<sub>2</sub>SO<sub>4</sub> is 10<sup>3</sup> M, allowing the same simplification to be made.

Many gases behave as weak acids in aqueous solution. Having a dissociation constant of 10<sup>-2</sup> mole l<sup>-1</sup>, a substantial part can stay in the undissociated form within the pH range typical for atmospheric particles. CO<sub>2</sub>, SO<sub>2</sub>, carboxylic acids, HONO and H<sub>2</sub>O<sub>2</sub> are all weak acids. Formaldehyde undergoes hydrolysis in the solution, forming methylene glycol, H<sub>2</sub>C(OH)<sub>2</sub>. The hydrolysis equilibrium constant is high (2530 at 298K, Seinfeld and Pandis, 1998) and all HCHO can be assumed to exist in the diol form. The dissolved hydroperoxy radicals behave also as weak acids, forming O<sub>2</sub><sup>-</sup> and H<sup>+</sup>.

Ammonia (NH<sub>3</sub>) is the only important base in the gas phase. When entering into a solution, it behaves as a weak base and dissociates to NH<sub>4</sub><sup>+</sup> and OH<sup>-</sup>.

The OH radical is an important oxidising species also in the aqueous phase. In addition to radicals transported from the gas phase, it is produced *in situ* by photolysis of H<sub>2</sub>O<sub>2</sub>, and by reaction of the O<sub>2</sub><sup>-</sup> radical with ozone. Photodissociation of NO<sub>3</sub><sup>-</sup>, NO<sub>2</sub><sup>-</sup>, HNO<sub>2</sub>, and oxidation of S(IV) by HO<sub>2</sub> are less important sources (Seinfeld and Pandis, 1998). Another important radical in aqueous solution is O<sub>2</sub><sup>-</sup>, which is involved in reactions with ozone, hydrogen peroxide and with a number of radical species, such as NO<sub>3</sub> and SO<sub>5</sub><sup>-</sup>. The nitrate radical



(NO<sub>3</sub>) is highly soluble (Table 9 in Paper IV), and it is transported to the droplets from the gas phase. During nighttime it is an important oxidising species in aqueous phase.

S(IV) in the aqueous phase can be oxidised by reactions with ozone and with H<sub>2</sub>O<sub>2</sub>. The reaction with O<sub>3</sub> is strongly pH dependent and it dominates over the H<sub>2</sub>O<sub>2</sub> oxidation pathway at pH above 5. In a fresh sea-salt solution, the oxidation of S(IV) by O<sub>3</sub> is the dominant path, while in aged sea-salt droplets with lower pH, the oxidation by HOBr and HOCl become more important (Keene *et al.*, 1998, Paper IV). The OH radical starts an oxidation chain of S(IV) (3.3), (3.4) (Huie and Netta, 1987), resulting in formation of an SO<sub>3</sub><sup>-</sup> radical in the first step, followed by a propagating mechanism (3.5) through (3.8). Formation of SO<sub>3</sub><sup>-</sup> in (3.7) and (3.8) are the propagating steps. The same mechanism can also be started by the NO<sub>3</sub> radical reaction yielding SO<sub>3</sub><sup>-</sup> and NO<sub>3</sub><sup>-</sup>.



The reaction rate coefficients are usually expressed in s<sup>-1</sup>, l moles<sup>-1</sup> s<sup>-1</sup>, or l<sup>2</sup> moles<sup>-2</sup> s<sup>-1</sup> for first, second, and third order reactions, respectively. Concentration units related to the air volume (in cm<sup>3</sup>) are used in the model calculations in order to handle the mass-transport problem. An aqueous rate coefficient RC<sub>air</sub> related to the air volume (in (molecules<sup>-1</sup> cm<sup>3</sup><sub>air</sub>)<sup>ro</sup> × s<sup>-1</sup>, where ro is the order of reaction) has to be calculated from the aqueous phase-related RC<sub>aq</sub> rate coefficients (in moles<sup>-ro</sup> × l<sup>ro</sup> × s<sup>-1</sup>) according to (3.10).

$$\text{RC}_{\text{air}} = \text{RC}_{\text{aq}} \times 1/(\text{N}_A \times \text{l}_s \times 10^{-3})^{\text{ro}} \quad (3.10)$$

(N<sub>A</sub> is Avogadro's number, 6.022 × 10<sup>23</sup> molec. cm<sup>-3</sup>).

### 3.1. Chemistry of sea-salt particles

The average composition of seawater is given in Table 2. Chloride ions are the most abundant anions in seawater, making up 97% on a molar basis. 0.3% of the anions are carbonate and bicarbonate anions, which are the main reason for the high pH of the sea-salt solution. The average seawater with a salinity of 35 ‰ has a pH of 8.1 at 25°C (Millero and Sohn, 1992).

A seawater droplet ejected into the atmosphere rapidly establishes equilibrium with the air humidity. The deliquescent point of NaCl is 75% RH. If the RH increases and reaches the deliquescent point, a dry salt particle would suddenly start to dissolve, forming a saturated solution. When the RH decreases from a value above the deliquescence point, the salt droplet often stays liquid even after passing the deliquescent point, thus becoming supersaturated.

**Table 2.** Composition of the mean seawater (from Millero and Sohn, 1992):  $M_i$  molecular weight,  $N_i$  molar fraction of species.

Species	$M_i$ $\text{g mol}^{-1}$	$N_i$
$\text{Na}^+$	22.99	0.8373
$\text{Mg}^{2+}$	24.31	0.0943
$\text{Ca}^{2+}$	40.08	0.0184
$\text{K}^+$	39.10	0.0182
$\text{Sr}^{2+}$	87.62	0.0002
$\text{Cl}^-$	35.45	0.9746
$\text{SO}_4^{=}$	96.06	0.0504
$\text{HCO}_3^-$	61.02	0.0033
$\text{Br}^-$	79.90	0.0015
$\text{CO}_3^{=}$	60.01	0.0003
Sea-salt	62.79	1.00

When the supersaturation is sufficient, crystallisation occurs and the water evaporates (Tang and Munkelwitz, 1993). Both experiments and observations show that sea-salt particles often stay as a supersaturated liquid down to around 40% RH (Cohen *et al.*, 1987, Rood *et al.*, 1989, Tang, 1997). These facts were the reason for including calculations with a supersaturated solution in Paper IV.

Chemical and volumetric properties of concentrated solutions are affected by solute interactions and activities  $a_i$ , rather than concentrations, have to be used in chemical calculations. Activities are calculated by multiplying concentrations by an activity coefficient. If concentrations are on a molal scale  $m$ ,  $a_i$  equals  $\gamma_i \times m_i$ , if they are on a molar scale  $M$ ,  $a_i$  equals  $\gamma_i \times M_i$ . Pitzer's equations are commonly used to calculate the activity coefficients of strong electrolytes (Pitzer, 1991). The computer programme PHRQPITZ (Plummer *et al.*, 1988) encodes Pitzer's equations and an extensive database of ion-interaction parameters  $\beta^{(0)}$ ,  $\beta^{(1)}$ ,  $\beta^{(2)}$ , and  $C^\phi$ , and of thermodynamic properties is included in the programme. Details of calculations of the activity coefficients are given in Paper IV. Activity coefficients  $\gamma$ , relevant for the sea-salt solution at different RH are listed in Table 10 in Paper IV.

Halogens can be released from the sea-salt particles by several mechanisms. The already mentioned expulsion of less soluble HCl by more soluble acids AH ( $\text{H}_2\text{SO}_4$  and  $\text{HNO}_3$ ), as defined by effective Henry's law constants, is the main mechanism of release of chlorine from the aqueous phase.



In the following, X will be used to designate Cl or Br. Hydroxyl radicals equilibrate with  $\text{X}^-$  in the sea-salt solution to form  $\text{XOH}^-$  (Jayson *et al.*, 1974, Klänning and Wolf, 1985).  $\text{XOH}^-$  ions enter into equilibrium with  $\text{H}^+$  and atomic halogens (Jayson *et al.*, 1974, Klänning and Wolf, 1985). Reaction sequence (3.13) and (3.14) is an important sink of aqueous OH

(Mozurkewich, 1995).  $\text{Cl}^-$  and  $\text{Br}^-$  and the corresponding halogen atom equilibrate to form dihalide anions  $\text{Cl}_2^-$  and  $\text{Br}_2^-$  (reaction 2.17). Since the equilibria favour  $\text{X}_2^-$  in the seawater,  $\text{X}_2^-$  is more important as oxidising agent than the halogen atoms. Self-reaction (3.16) leads to the formation of molecular halogens (Jayson *et al.*, 1974, Klänning and Wolf, 1985). Since  $\text{X}_2$  may easily evaporate, equilibria (3.13), (3.14), and (3.15), followed by reaction (3.16) is a possible mechanism of the halogen release, though the importance of this pathway is rather limited.



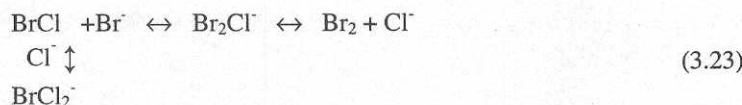
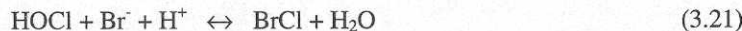
$\text{Br}^-$  and  $\text{Cl}^-$  can also be oxidised by dissolved nitrate radicals (Neta *et al.*, 1990), forming atomic halogens and  $\text{NO}_3^-$ , and by the radical species formed in the OH-initiated sulphur oxidation chain (reaction 3.17 - Neta *et al.*, 1990, reaction 3.18 for Cl - Jacob, 1986, for Br - Mozurkewich, 1995).



The reversible disproportionation of molecular halogens form hypohalogenous acid HOX, and  $\text{X}^-$  (reaction 3.19). The hydrolysis is acid-base assisted and the effect of acids AH present in the solution can be described by reversible reaction (2.20) (Wang and Margerum, 1994, Beckwith *et al.*, 1996).



The cross-reactions of hypohalogenous acid with halogen anions lead to the formation of bromide-chloride (BrCl), as described by reactions (3.21) and (3.22) (Kumar and Margerum, 1987, Vogt *et al.*, 1996). BrCl is equilibrated with  $\text{BrCl}_2^-$ ,  $\text{Br}_2\text{Cl}^-$ , and through  $\text{Br}_2\text{Cl}^-$ , also with  $\text{Br}_2$  (equilibria 3.23) (Wang *et al.*, 1994).

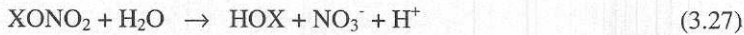


Formation of BrCl *via* the HOBr +  $\text{Cl}^-$  reaction (3.22), followed by equilibria towards  $\text{Br}_2$  (3.23), is part of the mechanism of autocatalytic bromine activation, proposed by (Vogt *et al.*, 1996). The dissolved  $\text{Cl}_2$  reacts irreversibly with  $\text{Br}^-$  in a fast rate, resulting in formation of  $\text{BrCl}_2^-$  (Wang *et al.*, 1994). As the reaction is followed by the equilibria in (3.23), any  $\text{Cl}_2$  formation in the aqueous phase is an efficient pathway of molecular bromine release.

Dinitrogen pentoxide ( $\text{N}_2\text{O}_5$ ), transported into the seawater droplets can either hydrolyse (3.24), or react with  $\text{Cl}^-$  (3.25) or  $\text{Br}^-$  (3.26). According to Behnke *et al.* (1994) and Behnke *et al.* (1997), only a small part is hydrolysed to nitric acid and the reaction with  $\text{Cl}^-$  dominates even in dilute sea-salt solutions. The formation rate of  $\text{BrNO}_2$  was assumed to be that of  $\text{ClNO}_2$ , scaled by the  $[\text{Br}^-]/[\text{Cl}^-]$  ratio.



Chlorine and bromine nitrates, formed in the gas-phase from  $\text{NO}_2$  and  $\text{ClO}$  or  $\text{BrO}$ , can dissolve into the particles and hydrolyse.



The reactive uptake of  $\text{XONO}_2$  on solid particles can also lead to the reaction with halogen anion  $\text{X}^-$  (Finlayson-Pitts *et al.*, 1989), resulting in formation of  $\text{X}_2$ . It has been speculated that the same mechanism is possible in the liquid phase (Sander and Crutzen, 1996).



The rate constants of reactions described in this chapter can be found in Table 11 in Paper IV.





## 4. Photolysis rates

The energy  $E$ , carried by a photon is given by relation 4.1.

$$E=hc/\lambda \quad (4.1)$$

$h$  is Planck's constant,  $c$  is the speed of light, while  $\nu$  and  $\lambda$  is the frequency and wavelength of the radiation, respectively.

A molecule may absorb a photon only if a process requiring exactly the energy of the photon can take place. Processes of interest for atmospheric chemistry involve an electronic transition combined with vibrational and rotational transitions. The energy needed often corresponds to light in the UV and visible regions. An excited molecule may undergo chemical change, or lose energy by radiative and non-radiative processes. The chemical processes could e.g. be molecular rearrangement or dissociation. The fraction of absorbed photons leading to a certain process is known as the primary quantum yield  $\Phi$  for that process. Absorption by  $N_2$ ,  $O_2$  and  $O_3$  in the upper atmosphere removes short wavelength sunlight and no light with a wavelength shorter than 290 nm needs to be taken into account at the Earth's surface.

Beer's law (4.2) describes the absorption of monochromatic radiation by a weakly absorbing medium.

$$I = I_0 \exp(-\sigma_{ABS,i} c l) \quad (4.2)$$

$I_0$  is the intensity of the incident radiation,  $I$  is the intensity of light after travelling a distance  $l$  through the medium,  $c$  is the concentration of the absorbing molecule and  $\sigma_{ABS,i}$  is the absorption cross section, a quantity that is a function of  $\lambda$  and that is unique for each compound  $i$ .

Photolysis is of particular interest in atmospheric chemistry since it is often a source of free radicals. The photolysis rate of compound A may be described by a first order rate equation.

$$dc_A/dt = J c_A \quad (4.3)$$

The photolysis rate constant  $J$  is a function of photolysis quantum yield, absorption cross section and light intensity and may be derived from Beer's law giving expression (4.4).

$$J_i = \int_{\lambda_1}^{\lambda_2} \sigma_{ABS,i}(\lambda, T) \phi_i(\lambda, T) I(\lambda) d\lambda \approx \sum_j \sigma_{ABS,i}(\lambda_j, T) \phi_i(\lambda_j, T) I(\lambda_j) \Delta\lambda_j \quad (4.4)$$

$T$  is temperature and  $j$  denotes an average over a wavelength interval  $\Delta_j$  with a centre wavelength  $\lambda_j$ . Absorption cross sections  $\sigma_{ABS,i}$  and quantum yields for photolysis  $\phi_i$  of common atmospheric trace gases can be found in e.g. Atkinson *et al.* (1997) and DeMore *et al.* (1997). The photolysis quantum yield and absorption cross section are dependent on temperature and

wavelength while the light intensity is a function of solar zenith angle  $\Theta$ . The actinic fluxes, calculated by a multiple-layer model of atmospheric extinction of solar radiation have been published (e.g. Demerjian *et al.*, 1980, Madronich, 1987). The calculations account for the path-length of light through atmosphere, absorption by gases and aerosols, and for the back scattering by aerosols and molecules.

The solar zenith angle  $\Theta$  dependent photolytic rate coefficients can be expressed in a functional form convenient for model calculations.

$$J_i = A_i \times \exp(-B_i/\cos\Theta), \quad (4.5)$$

$A_i$  and  $B_i$  are parameters obtained by fitting the exponential function  $J_i$  to  $1/\cos\Theta$ . The actinic flux data of Demerjian *et al.* (1980) were used to calculate  $J_i(\Theta)$  in the calculations presented in this thesis.

The actinic flux in the liquid aerosol particles differs from that in the gas phase mainly due to the light scattering at the particle surface. This problem was addressed in a study by Ruggaber *et al.* (1997) who found, that the actinic flux in particles in the transition and continuum size regimes is enhanced approximately by a factor of 2 over the entire wavelength interval relevant for troposphere. This value was used in the calculations in Paper IV. The mean daytime values of the photolysis rate constants in the gas and aqueous phase, calculated for 57° N latitude, 21 August, are listed in Table 7 and 12 of Paper IV.

## 5. Transport processes

### 5.1. Exchange of mass at the gas-particle interface

Liquid particles may serve as a sink, source, or a reservoir of the active species. Raoult's law (5.1) describes the gas phase concentration  $c_i$  of compound  $i$  over a solution, where  $i$  is present at a molar fraction  $x_i$ , when the saturation concentration above pure  $i$  is  $c_{i0}$  and the activity coefficient of  $i$  in the mixture is  $\gamma_i$ . As  $x_i$  approaches 0,  $\gamma_i$  approaches 1.

$$c_i^{eq} = x_i \gamma_i c_{i0} \quad (5.1)$$

The equilibrium vapour pressure is preferably expressed by the Henry's law (3.1). The saturation concentration above the solution  $c_i^{eq}$  is related to the aqueous concentration  $c_{ia}$  (related to the air volume) through (5.2), derived from (3.1).

$$c_i^{eq} = x_i \gamma_i / (H_i RT) = c_{ia} \gamma_i / (H_i RTL), \quad (5.2)$$

$L$  is the dimensionless liquid solution content. The equilibrium vapour concentration  $c_{ij}^{eq}$  over very small particles with diameter  $D_{pj}$  is affected by the Kelvin effect,

$$c_{ij}^{eq} = c_i^{eq} \times \exp\left(\frac{4V_{mol}\sigma}{kTDp_j}\right). \quad (5.3)$$

In (5.3)  $V_{mol} = m_w / (\rho N_A)$  is the molecular volume,  $\rho$  is the density,  $N_A$  is Avogadro's number,  $m_w$  is the molar weight,  $\sigma_i$  is the surface tension of species  $i$ ,  $k$  is Boltzmann's constant, and  $T$  (K) is the temperature.

The net flux  $dc_{icj}/dt$  between the gas and condensed phase of species  $i$  in particle size interval  $j$  with diameter  $D_{pj}$  can be described by equation (5.4), which applies in all particle size regimes (Seinfeld, 1986).

$$\frac{dc_{icj}}{dt} = k_{ij} (c_i - c_{ij}^{eq}) = n_j 2\pi D_{pj} D_{gi} \beta(Kn) (c_i - c_{ij}^{eq}), \quad (5.4)$$

$k_{ij}$  is the transfer coefficient,  $n_j$  is number of particles in size interval  $j$ , and  $D_{gi}$  is the gas phase diffusivity of  $i$ . Details of calculations of  $D_{gi}$  are given in Paper IV and V.  $\beta(Kn)$  is an interpolation expression for the transition regime derived by the Fuchs' flux matching method.  $Kn = 2\lambda/D_{pj}$  is the Knudsen number.

$$\beta(Kn) = \frac{1 + Kn}{1 + \frac{3\pi}{8} (1 + m_w / m_{w,air}) (Kn + Kn^2) \times 1/\alpha}, \quad (5.5)$$

$m_w$  and  $m_{w,air}$  are molecular weights of the condensing species and of air, respectively, and the dimensionless accommodation coefficient  $\alpha$  expresses the fraction of molecules that pass the gas-liquid boundary. The transfer coefficient expressed by equation (5.4) is employed in



calculations of the mass transport in Paper V. Schwartz (1986) developed a formula describing the transport between the gas phase and the aqueous droplets, which is widely used in atmospheric models, including the CCDSSP model. The transfer coefficient  $k_{ij}$  has the form

$$k_{ij} = L \times \left( \frac{Dp_j^2}{3D_g} + \frac{4Dp_j}{3\bar{c}\alpha} \right)^{-1} \quad (5.6)$$

The first part of the expression inside the brackets of equation (5.6) comes from the gas phase diffusion and the second part from the interfacial transport. Gases that do not dissolve well in the liquid often have  $\alpha$  values below 0.01 and those which do dissolve well have  $\alpha$  between 0.01 and 1. In the latter case the gas-phase diffusion term  $Dp_j^2/3D_g$  of equation (5.6) dominates over the  $4Dp_j/3\bar{c}\alpha$ , the rate is diffusion limited and the process shows very little sensitivity to the  $\alpha$  value (Lelieveld and Crutzen, 1991).

When a secondary product with low vapour pressure is formed by a reaction and its condensation rate is low, e.g. if few or no aerosol particles are present or if  $c_{i0}$  is very low, the gas phase concentration will increase with increasing supersaturation  $S = c_i/c_{i0}$  as a result. The gas-to-particle conversion may then take place *via* homogenous nucleation. The nucleation rate  $dn_{\text{(nucl)}}/dt$  (molec. unit volume<sup>-1</sup> s<sup>-1</sup>) can be calculated by the classical nucleation theory according to (5.7) (Oxtoby, 1992). The critical diameter of the nucleating particles,  $D_{p(\text{crit})}$  defines the size of new particles formed according to (5.8).

$$\frac{dn_{\text{nucl}}}{dt} = \left( \frac{2\sigma N_A}{\pi n_w} \right)^{1/2} V_{\text{mol}} (c_i^{\text{eq}})^2 S \times \exp \left( -\frac{16\pi}{3} V_{\text{mol}}^2 \left( \frac{\sigma}{kT} \right)^3 \left( \frac{1}{\ln S} \right)^2 \right) \quad (5.7)$$

$$D_{p(\text{crit})} = 4V_{\text{mol}} \left( \frac{\sigma}{kT \ln S} \right) \quad (5.8)$$

## 5.2. Limitation of reaction rates by aqueous phase diffusion

The lifetime of OH and some other rapidly reacting species in the liquid is of the same order of magnitude or shorter than the characteristic time of diffusion in the aqueous phase (Lelieveld and Crutzen, 1991), which implies that the reaction rate of OH is limited by mass transport. The average concentration of OH in a droplet is related to the surface concentration through

$$Q = [\overline{\text{OH}}]/[\text{OH}]_{Dp} = 3 \times \left( \frac{\coth q}{q} - \frac{1}{q^2} \right) \quad (5.9)$$

(Schwartz 1986), where  $[\overline{\text{OH}}]$  is the bulk concentration and  $[\text{OH}]_{Dp}$  is the concentration at the particle surface.  $q$  is a dimensionless diffuso-reactive parameter given by

$$q = Dp \times \left( \frac{k^{(1)}}{D_a} \right)^{1/2} \quad (5.10)$$

$k^{(1)}$  is the first order reaction rate constant of OH and  $D_a$  is the aqueous phase diffusion constant of OH, a typical value of which is  $2.0 \times 10^{-5} \text{ cm}^2 \text{ s}^{-1}$  (Lelieveld and Crutzen, 1991).  $Q$  in Equation (5.9) applies only to the part of OH that is transported to the droplet and not to the part, that is formed in the particle, i.e. by  $\text{H}_2\text{O}_2$  photolysis. OH reaction rates in aqueous phase are then corrected for the aqueous diffusion limitation by a factor  $Q' = 1 \times \text{OH}_{\text{is}} / \text{OH}_{\text{tot}} + Q \times \text{OH}_{\text{tr}} / \text{OH}_{\text{tot}}$ , where  $\text{OH}_{\text{is}}$  and  $\text{OH}_{\text{tr}}$  are the OH radicals formed *in situ* in the solution and transported into the solution, respectively and  $\text{OH}_{\text{tot}} = \text{OH}_{\text{is}} + \text{OH}_{\text{tr}}$ .

### 5.3. Fluxes and concentrations of sea-salt particles

Solar energy, wind, and gravitational forces drive mass exchange between the sea and air. The flux of seawater particles to the atmosphere and their return back to the ocean determine the concentration and size distribution of the sea-salt aerosol. Seawater is ejected into the atmosphere by bursting bubbles, which produces two types of particles. Each bursting bubble gives 1-10 jet droplets with a diameter of around 10-20  $\mu\text{m}$ , and many small film particles with diameters ranging from less than 1  $\mu\text{m}$  to about 5  $\mu\text{m}$ . Large particles with diameters of several hundreds of  $\mu\text{m}$  and up to centimetre size are created by tearing of water from the wave whitecaps (Blanchard and Woodcock, 1980). Large particles have high settling velocity and exist only seconds before they fall back to the sea. Only small particles can be transported to higher altitudes by turbulence and convection.

An increasing wind velocity affects several processes in the sea-salt aerosol production. Breaking waves mix more bubbles into the water and also more spume droplets are torn from the wave whitecaps. Therefore, more particles are produced at higher wind-speed, especially at the large size side of the particle-size distribution spectrum. At the same time, wind can drift larger particles to higher altitudes. It follows, that concentration and particle size distribution of the sea-salt particles in the marine troposphere varies strongly with wind speed and altitude (Woodcock, 1953, Junge, 1957, Lovett, 1978). Close to the sea surface, at wind speeds around 10 m/s, the sea salt concentrations are typically 10 - 20  $\mu\text{g}/\text{m}^3$ . For wind-speeds of 15 m/s Lovett (1978) gives a range of values from 40 to 74  $\mu\text{g}/\text{m}^3$  (altitude 5-15 m). Generally, the sea-salt concentrations in the marine boundary layer decrease with increasing altitude and the vertical gradient decreases with decreasing wind speed (Blanchard and Woodcock, 1980).

Kim *et al.*, (1990) measured sea-salt particle size distributions off the US East Coast and at the Bermudas and fitted them to a log normal aerosol size distribution, as described in Paper IV. These distributions, measured at wind-speeds of 4 and 10  $\text{m s}^{-1}$ , were used for the sea-salt aerosol simulations in Paper IV.

The sea-salt concentrations in surf regions are substantially higher than those measured above the free ocean. Relation (5.13) between sea-salt concentration  $Sc$  (in  $\mu\text{g}/\text{m}^3$ ) and wind

speed  $u$  (in m/s) has been derived from measurements at the Cumbrian coast by McKay *et al.* (1994):

$$\ln(\text{Sc}) = 0.23u + 3.05 \quad (5.13)$$

In the model calculations in Paper IV, the total aerosol volume was reduced by 1/3 in order to account for the fact that the data were collected close to the bottom of the boundary layer while the calculations concern the entire boundary layer. Figure 1 compares the dry aerosol size distributions at 4 and 10 m/s wind-speeds over the free ocean and at the coast. Parameters of the marine and tidal aerosol size distributions can be found in Table 1 in Paper IV.

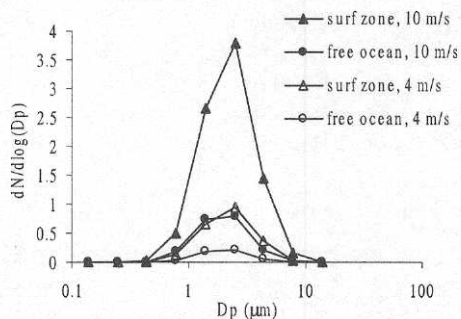


**Figure 1.** The particle size distributions of the dry sea-salt aerosol at two different windspeeds, 4 and 10 m s<sup>-1</sup>, used in the CCDSSP model (Paper IV).

#### 5.4. Deposition

Deposition is the ultimate removal process of gases and particles from the atmosphere. It may take place either by interaction with surfaces on ground, as a dry deposition, or by washout by precipitation, as a wet deposition. The wet deposition was not studied in this work and thus, in the following, the dry deposition is meant when the term “deposition” is used. The flux of depositing species  $i$  ( $i$  is a gas or a particle), depends on the concentration  $c_i$  and can be described by Equation (5.14).

$$F_i = c_i \times v_{di} \quad (5.14)$$

$v_{di}$  is the dry deposition velocity. As concentrations usually have a gradient above the surface, the dry deposition velocity is height dependent. The deposition is generally controlled by three processes. Firstly, transport of the species from atmosphere to the very thin surface layer, called the interfacial or quasi-laminar sub-layer, is driven by turbulent motion of the air, and, in the case of larger particles, also by sedimentation. Secondly, transport through the interfacial layer to the surface is driven by molecular (gases) or Brownian (small particles) motion with a contribution of sedimentation (large particles). Thirdly, uptake of species at the surface depends both on the character of the surface, and on properties of the deposited material. Gases can be absorbed reversibly or irreversibly and some gases, as e.g. ozone, can also be taken up by vegetation through the stomata. Particles can adhere on the surface. Each of the three processes contributes to the deposition velocity. A common way of

describing the deposition process is using an analogy with electric resistance  $R$ , defining  $R = v_d^{-1}$  and  $1/v_d = R_T = R_{SL} + R_{IL} + R_C$ , where subscripts T, SL, IL, and

**Table 3** Dry deposition velocities of gaseous species used in the model (partly from Sander and Crutzen, (1996), partly estimates). The lower ozone deposition value (\*) applies during the nighttime.

Species	$v_d$ land	$v_d$ sea surface
	m/s	m/s
HNO <sub>3</sub>	200	50
N <sub>2</sub> O <sub>5</sub>	200	50
SO <sub>3</sub>	200	100
NO <sub>3</sub>	100	50
H <sub>2</sub> O <sub>2</sub>	100	50
HCHO	100	50
HCO <sub>2</sub> H	100	50
SO <sub>2</sub>	100	50
NO <sub>2</sub>	60	10
O <sub>3</sub>	4* - 100	4
OH	100	100
HO <sub>2</sub>	100	100
XO <sub>2</sub>	50	50
CH <sub>3</sub> O <sub>2</sub> H	50	50
NH <sub>3</sub>	30	30
HOCl	20	20
HOBr	20	20
HCl	100	50
HBr	100	50
org. nitrates	20	10

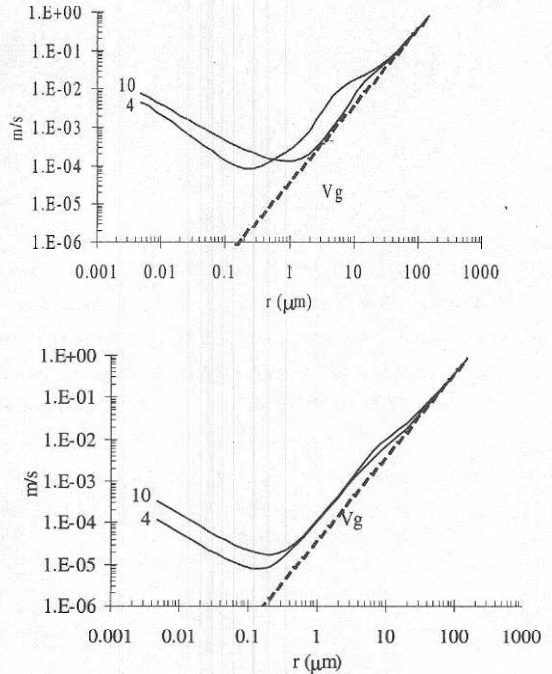


**Figure 2** Size dependent deposition velocities of the sea-salt particles a) on canopy surface, calculated by equation XI and X in Paper V after Giorgi, (1986) and b) on sea-surface, calculated by equation VII and VIII in Paper V after Slinn and Slinn, (1980). The relative humidity in the surface layer is 80%.

C stands for the total, surface sub-layer, interface sub-layer, and canopy resistances, respectively. Since these resistances are serial, the largest resistance will limit the total deposition.

Models used in Paper II, III and IV distinguish between deposition velocities on water and on land. The deposition velocities of gaseous species are presented in Table 3. The size-dependent particle deposition velocities are shown in Figure 2. Details of the 2-layer deposition model used in Paper IV can be found in the Paper.

The change of concentration  $c_i$  within the planetary boundary layer of thickness  $H_{mix}$  due to the deposition can be described by equation (5.15).



$$dc_i/dt = v_{di} \times c_i/H_{\text{mix}}. \quad (5.15)$$

Experimental studies of the air pollution problems are often performed in experimental reactors of various shapes, sizes, and materials. Deposition on reactor walls is then a common problem, which needs to be addressed especially when particles are concerned. The total deposition rate ( $s^{-1}$ ) can be computed from the local deposition flux and the internal surface of the chamber. The deposition coefficient  $\beta_{\text{dep}}$  ( $s^{-1}$ ) defined for particle deposition in a spherical reactor of radius  $R$  is given by Crump and Seinfeld (1981).

$$\beta_{\text{dep}} = \frac{6\sqrt{k_e D}}{\pi R} Df\left(\frac{\pi v_g}{2\sqrt{k_e D}}\right) + \frac{v_g}{4R/3}, \quad (5.16)$$

$k_e$  is the turbulent diffusivity coefficient,  $D$  is the Brownian diffusivity of the particle, and  $Df$  is the Debye function, defined by Crump and Seinfeld (1981). The second term in (5.16) results from the gravitational settling of particles while the first term comes from the diffusion. As indicated by equation (5.16), the deposition coefficient  $\beta_{\text{dep}}$  is size-dependent. The greatest problem in estimation of the deposition coefficient is the magnitude of the turbulent diffusivity coefficient  $k_e$ . One experimental possibility is filling the reactor with aerosol particles and fitting the measured concentration time series to calculations, involving particle deposition and coagulation. Figure 3 shows the particle size-dependent deposition coefficient  $\beta$  calculated for the reactor chamber described in Paper V, using different  $k_e$ 's.

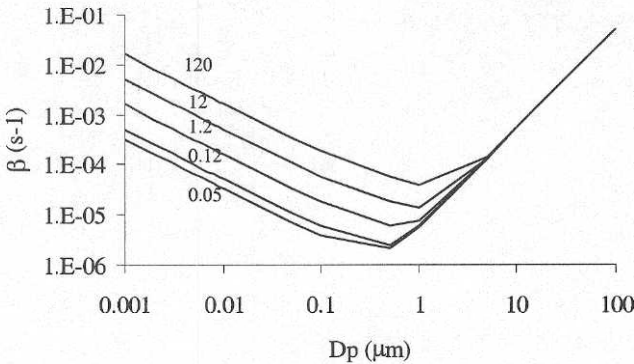


**Figure 3** Deposition coefficients  $\beta_{\text{dep}}$  for the reactor described in Paper V, calculated for diffusivity coefficients  $k_e$  given by the figures next to the lines.

## 6. Mathematical description

### 6.1. Analysis of measured concentrations

The basic descriptive statistical analysis of measurements is the first step in processing of a data set. If the frequency distribution is skewed, a logarithmic transformation of the data must precede further calculations. Ambient concentrations often exhibit a strong seasonal trend and the descriptive statistic has to be performed either on stratified data, or the data have to be filtered by a seasonality function prior to the analysis. An example of the first method is given in Paper I, where the concentration data are analysed on a monthly basis, giving each month the same weight in further calculations.

Analysis of variance of the data helps to recognise significant processes affecting the concentrations. A multivariate analysis of variance (MANOVA), used in Paper I, separated individual sources of variability in the data set. If two factors,  $i$  and  $j$ , having  $n$  and  $m$  levels, respectively, affect concentrations, then  $n \times m$  factor levels can be defined in the data set. E.g. if  $i$  is the effect of the season and  $j$  is the effect of the origin of the air mass, and if we define factor levels  $n = 12$  (months) and  $m = 4$  (N, E, S, W), then the total number of factor levels is 48. A linear additive statistical model was applied to the data, i.e. the mean  $\mu_{ij}$  of each factor level was calculated according to equation (6.1) (Netter *et al.*, 1990).

$$\mu_{ij} = \mu_g + \alpha_i + \beta_j + \alpha\beta_{ij} \quad (6.1)$$

$\mu_g$  is the overall mean,  $\alpha_i$  is the mean effect of the  $i^{\text{th}}$  factor,  $\beta_j$  is the mean effect of the  $j^{\text{th}}$  factor and  $\alpha\beta_{ij}$  is the mean for interaction between the  $i^{\text{th}}$  and  $j^{\text{th}}$  factor. The meaning of "interaction" can be explained by the previously used example:  $\alpha\beta_{ij}$  is statistically significant when the mean effect of transport sector  $j$  varies throughout the year and is equal to the difference between  $\beta_j$  and the mean effect of transport sector  $j$  in month  $i$ . An important presumption in using this kind of analysis is having a reasonable theory which would be either verified or rejected by the analysis. Seasonal, diurnal and spatial variability was investigated on 9 VOC species and ozone in Paper I. The seasonal variability was studied by dividing year to months. The diurnal variability was studied for 6 points during the day, according to the measuring schedule at Rörvik. For studying spatial variability, 96-hour back-trajectories were calculated for each measurement of the two years period. The trajectories were calculated using winds at the 925-mb level from the numerical weather prediction model at the Norwegian Meteorological Institute.

An example of the data interpretation is presented in Paper I, where the drop in concentrations of individual hydrocarbons in spring was calculated as if it was caused solely by increase of the OH concentration. Comparison of calculations with measurements may give an indication whether this is the case or not. Laboratory data are, in contrast to ambient measurements, the result of reasonably well-controlled processes. The data interpretation is therefore much more straightforward and even if many parameters are unknown, indirect

estimates are often possible. In Paper V, apparent vapour pressures of condensing species were estimated from series of experiments with different amounts of produced condensable matter. These estimates were derived directly from Raoult's law and from the gas-to-particle partition equations presented in the Paper. During the same experiments, measurements of the development of total particle concentration gave information about the rate of nucleation of the new particles in the system. The nucleation rate is a function of supersaturation, and hence of the equilibrium vapour pressure, of the nucleating species (Equation 5.7). However, several other physical properties, such as surface tension and molecular weight are also to a great extent affecting the nucleation rate. Since not only the properties, but also the identity of the condensing matter itself was unknown, the nucleation function was used only as a way of parametrising the nucleation rather than a true physical description of the process.

## 6.2. Numerical models

The models developed and described in this work are in general of Lagrangean type, i.e. models, where an air parcel follows a trajectory above the Earth surface and the boundary conditions are defined along this trajectory. The particle formation model described in Paper V is a box model, which can be understood as the simplest case of the Lagrangean model, where both emissions and deposition are zero. The mixing ratio  $c_i$  of gaseous species  $i$  in an air parcel containing aerosol particles with particle diameters divided into size categories  $j$  can be described by

$$\frac{dc_i}{dt} = P_g - S_g + \frac{Q_g}{h} - \frac{D_g}{h} - \sum_j [k_{i,j}(c_i - c_{i,j}^{eq})] - n_{nucl} N_{(crit)}. \quad (6.2)$$

$P_g$  and  $S_g$  are the gas phase chemical production and loss terms respectively,  $Q_g$  and  $D_g$  are the emission and deposition fluxes and  $h$  is the height of the tropospheric boundary layer. The last two terms in (6.2) applies only when particulate matter is present. The interfacial transfer coefficient  $k_{i,j}$  can have different forms (Equations 5.4 to 5.6).  $c_{i,j}^{eq}$  is the equilibrium gas phase mixing ratio of component  $i$  above the liquid particle. If the Kelvin effect (Equation 5.3) is neglected,  $c_{i,j}^{eq}$  equals  $c_i^{eq}$  according to Henry's or Raoult's law (Equations 5.1, 5.2). The nucleation term was used only in the secondary aerosol formation model (Paper V) and  $N_{(crit)} = \pi/6 D_{p_{crit}}^3 V_{mol}^{-1}$  is the number of molecules in the critical cluster at homogenous nucleation (Equations 5.7, 5.8). In the last model mentioned, emission and deposition terms  $Q_g$  and  $D_g$  were zero and simulations were initiated with concentrations of reacting gaseous species. Concentration in the bulk condensed phase  $c_{i,a}$  is described by

$$\frac{dc_{i,a}}{dt} = P_a - S_a + \frac{Q_L x_{i,s}}{h} - \frac{D_L x_i}{h} + \sum_j k_{ij}(c_i - c_{i,j}^{eq}) + n_{nucl} N_{(crit)}. \quad (6.3)$$

$P_a$  and  $S_a$  are the aqueous phase chemical production and loss terms, respectively,  $Q_L$  and  $D_L$  are emission and deposition fluxes of the aerosol solution and  $x_{i,s}$  and  $x_i$  are molar fractions of

species  $i$  in newly injected and reacted particle solution, respectively. In the secondary aerosol particle formation model, the continuity equation for the condensed phase is particle size-resolved and the coagulation process is included. This brings about a problem, since both number and mass of the aerosol particles changes due to these two processes. Particle size resolved equations and a solution to this problem are described in detail in Paper V. The CCDSSP model is quasi-size dependent, which means that the air-particle exchange and deposition are particle size-resolved, while the chemical reactions are treated for the bulk solution.

The mass conservation equations for species  $i$  (6.2) and (6.3) can be rewritten in a form common for both gas and condensed phases with all sources gathered in the term  $Q_{i,tot}$  and all sinks in the term  $S_{i,tot}c'_i$  ( $c'_i$  is concentration in gas or aqueous phase).

$$\frac{dc'_i}{dt} = Q_{i,tot} - S_{i,tot}c'_i(t). \quad (6.4)$$

Both terms on the right hand side of (6.4) depend on concentration of other species, which results in a system of ordinary differential equations. The system is most often so complex, that an analytical solution is not possible and numerical solutions are necessary. A common problem found in atmospheric chemistry calculations is that the system described by Equation 6.4 is stiff, i.e. value of  $c_i$  changes only slowly, while the sink and source terms are large and almost cancel each other. The ratio between  $S_{i,tot}$  and relative rate of the change of  $c_i$ ,  $(1/c_i)dc_i/dt$ , is called the degree of stiffness. Choice of a time-step resulting in a small, but not too small  $(1/c_i)dc_i/dt$ , giving a stiffness ratio  $(S_{i,tot}\Delta t)_{max}$  lower than a defined value, is one method of solving this problem. Gear's method is such an algorithm suitable for solving stiff equation systems described by (6.4) (Curtis and Sweetenham, 1987). In models described in Paper II and IV, the FACSIMILE program, employing Gear's method (AEA, 1994), was used to solve the equations.

Equation 6.4 can also be solved by evaluating the ratio between the time-step  $\Delta t$  and the natural lifetime of species  $i$ ,  $\tau_i$ , defined as  $1/S_{i,tot}$ . If  $\Delta t \ll \tau_i$ , Equation 6.4 can be solved by Euler's formula:

$$c_i(t_0 + \Delta t) = c_i(t_0) + (Q_{i,tot} - S_{i,tot}c_i(t_0))\Delta t, \quad (6.5)$$

While for  $\Delta t \gg \tau_i$ ,  $c_i$  tends to attain a steady-state concentration and  $c_i(t_0 + \Delta t) = Q_{i,tot}(t_0 + \Delta t)/S_{i,tot}(t_0 + \Delta t)$ . For time-steps similar to the lifetime, under an assumption of constant sink and source rates during the time-step, an analytical solution of Equation 6.4 can be used.

$$c_i(t_0 + \Delta t) = \frac{Q_{i,tot}}{S_{i,tot}} + \left[ c_i(t_0) - \frac{Q_{i,tot}}{S_{i,tot}} \right] \exp(-S_{i,tot}\Delta t) \quad (6.6)$$

(Hesstvedt *et al.*, 1978). Euler's formula (6.5) in combination with small enough time-steps was used for solution of the mass conservation equations in the secondary particle formation model (Paper V).





## 7. Results and discussion

### 7.1. Concentrations of NMHC and ozone

A detail account of the work referred to in this section is given in Papers I and II. Data from the Rörvik background monitoring station for the period between February 1989 and October 1990 were analysed and used for comparison with model calculations. Hydrocarbon concentrations were sampled 6 times a day during a 20 minutes period every fourth hour, using an automatic gas chromatographic system (Mowrer and Lindskog, 1991). Concentrations of 9 hydrocarbon species (ethane, propane, isobutane, n-butane, isopentane, n-pentane, ethene, propene, and acetylene) were evaluated. Ozone data were measured continuously during this period.

The basic descriptive statistics applied to the data shows considerable differences between the hydrocarbon species. The frequency distributions of ethane and propane concentrations have a pronounced bimodal shape, the mode with the lower and the higher mean corresponding to concentrations in summer and winter seasons, respectively. The frequency distribution of acetylene shows a similar phenomenon, but as means of the two modes are closer, the data are more overlapping (Figure 1, Paper I). Other species have skewed lognormal distributions. The data time series presented in Paper I show, that the generally very scattered concentrations are low during summer and high during winter, as can be expected from the known photochemical processes involved in oxidation of NMHC. The correlation matrix indicates a rather high correlation between all measured NMHC species with a lower negative correlation to ozone concentration. Among the NMHC species, three groups with a higher internal correlation can be found. Ethane and propane, having the highest correlation, followed by butanes correlated with pentanes, and ethene with propene. Acetylene did not correlate very well with the other compounds. Seasonal, diurnal and spatial variances were studied for the four NMHC categories and for ozone. Variations both over seasons, origin of the air masses, and over the day were found to be statistically significant. Interactions between variation with seasons and with origin of the air masses were significant in the hydrocarbon data, while in ozone data all interactions were significant on the 5% level.

The seasonal variation of ozone concentration exhibits a minimum in winter and, after a rapid increase in concentration during the early spring, a broad maximum in the late spring and summer. Most NMHC species are negatively correlated to ozone. Their concentrations reach a minimum in summer and a maximum during winter months. At some other monitoring stations, a smaller summer maximum in the concentration of some hydrocarbons, such as ethene and propene, was observed. This was explained by biogenic emissions and their seasonal variation (Hov *et al.*, 1992). Different processes may contribute to the seasonal

variation. The VOC are lost through chemical reactions, initiated by important oxidising species, such as OH, O<sub>3</sub> or NO<sub>3</sub>, and concentrations of these species change throughout the year due to the seasonal variation in solar radiation intensity and concentrations of the precursors to these species. Some sources of VOC, both biogenic and manmade, have a seasonal variation. Also the large scale mixing can contribute to the seasonal variability e.g. by bringing the air from more southern latitudes to the North, where the air-masses, exposed to low photochemical activity, were rather isolated during the winter and could accumulated pollutants. As the chemical processes are concerned, the seasonal variation of species reacting at faster rate with OH is expected to be larger than that of long-lived species. As a result, the NMHC profile (i.e. the relative contribution of individual species to the total NMHC concentration) should have larger contribution from short-lived species in winter than in summer.

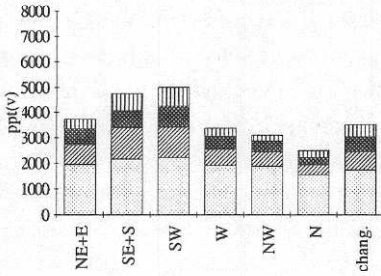
Theoretically, if two species with different reactivities are emitted at constant rates  $Q_i$  and are oxidised by the OH radicals, present at a constant concentration, the ratio between the two species can be derived from equation (6.6). When the reaction time is long enough, the exponential term in (6.6) approaches zero and the ratio between species 1 and 2 approaches  $Q_1/Q_2 \times k_2/k_1$  ( $k_i$  is the rate constant of the reaction between species  $i$  and OH), and becomes independent of the OH concentration. This is, however, seldom the case for the NMHC concentrations measured at Rörvik. Most often, a case where the NMHC are transported from polluted areas over the ocean, or other areas with little or no emissions, and undergo an exponential decay, may be expected. Calculations of the fast spring decay in concentrations of ethane and propane, employing a modified version of (6.6) (Paper I, p. 2396) showed, that the change in ratio between these two species can not be explained solely by the photochemistry and an influence of the hemispheric mixing was suggested.

The measurements were analysed with respect to the origin of the air mass as described in detail in Paper I. Large differences in composition were found between air masses of different origin. The highest concentrations were arriving from Central and Eastern Europe and the lowest from the northeast and from the west. The air masses arriving from westerly directions were highest in ozone concentrations, indicating an influence of aged polluted air masses transported from the UK to Sweden across the North Sea, where deposition rate of ozone was low. Concentrations of individual NMHC species in the air of different origin is shown for the four seasons in Figure 4 together with frequencies of the air mass origin and with concentrations of ozone.

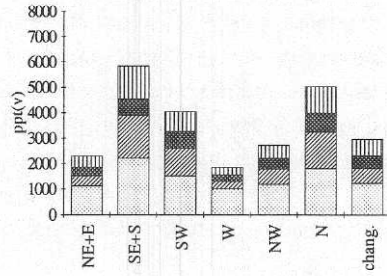
The measurements show a statistically significant diurnal variability of all NMHC species. This variability is, however, much less pronounced than that caused by season and by origin and there are no statistically significant interactions. The highest values were measured in the afternoon and the least pronounced maximum was that of ethane, the least reactive species. It was not possible to point out one process as a main reason of the diurnal variability. Different processes, which could cause this diurnal pattern, are discussed in Paper I.

The concentrations measured at Rörvik at the beginning of a spring episode with enhanced concentrations of NMHC, ozone and PAN were compared to model calculations in Paper II. The model was a Lagrangean trajectory model, involving only gas phase chemistry, with a detailed reaction scheme for oxidation of hydrocarbons. The model was described in

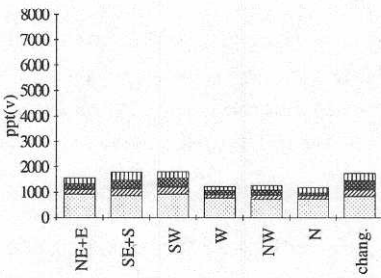
a) NMHC concentrations in spring



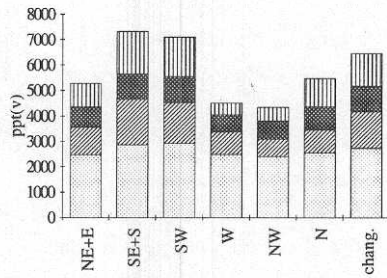
c) NMHC concentrations in autumn



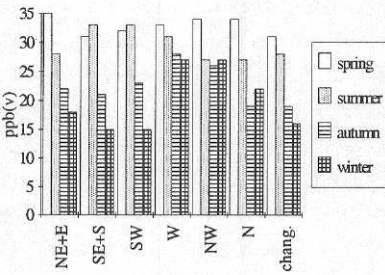
b) NMHC concentrations in summer



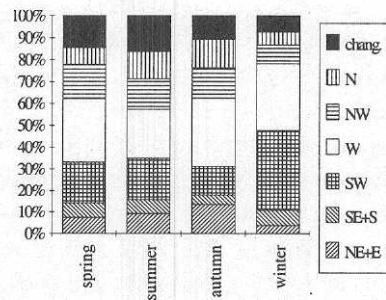
d) NMHC concentrations in winter







e) Ozone concentrations



f) Relative frequencies of transport situations



**Figure 4** Mean seasonal concentrations of some NMHC species (a, b, c, d, ethane , acetylene , n-butane , ethene ), ozone (e) associated with different sectors of the air mass origin. Relative frequencies of the transport sectors are shown in f.



detail e.g. in Moldanová (1994). The calculations generally reproduced concentrations of individual NMHC within a factor of two, but often much better, which was a satisfactory result if the simplifications made in the model were considered. A sensitivity study showed that the emission pattern had a major influence on the results. The influence of  $\text{NO}_3$  and Cl initiated oxidation of hydrocarbons on final NMHC concentrations was found to be of minor importance. Lagrangean models are more sensitive than Eulerian models to the emission pattern and intensity, because they neglect horizontal dispersion. As they are widely used e.g. for calculation of source-receptor relationships between the European countries and for calculations of secondary pollutant formation, the need for a detailed time and space-resolved emission inventory of both anthropogenic and natural emissions is obvious.

## 7.2. Halogen chemistry in the troposphere

A detail account of the work referred to in this and in the next section is given in Papers III and IV. The chemistry of halogen compounds in the troposphere was investigated with help of the CCDSSP (Coastal Chemistry and Deposition of Sea-Salt Particles) model, developed for the purpose of this study. Processes accounted for in the model are described in previous chapters and in Paper IV.

The "base case" run of the model simulates summer conditions with a windspeed of  $10 \text{ m s}^{-1}$ , 80% RH and clean background air (c.f. Table 13 in Paper IV). At the beginning of the simulation, particles are transported over the sea and production and deposition are in steady state.  $\text{SO}_2$  and  $\text{HNO}_3$  start to dissolve into the particles and their pH drops to a value of around 4 within the first hours of simulation. Since  $\text{O}_3$  and  $\text{NO}_3$  are present, radical reactions begin and the release of halogen species starts. No emissions of gaseous species takes place from the sea surface and the bulk pH increases slightly as the acidifying gases are gradually lost through the deposition and as the fresh particles, which have a pH close to 9, are mixed in. A new population of particles with a different size distribution is injected to the air parcel at the time of passage over the coast. Over land, the particles are deposited at a rate dependent on their size. Development of the particle size distribution during the base case simulation is shown in Paper IV, Figure 2. When the air parcel has passed the coast, emission of  $\text{SO}_2$  and oxides of nitrogen starts and HCl is driven out from the particles, being replaced mainly by  $\text{HNO}_3$  and  $\text{H}_2\text{SO}_4$ . The acidic compounds dissolve into the droplets or are produced *in situ*. The pH drops to 3.5 during the 3 days of simulation over land.

The calculations confirm that the reaction of HCl with OH (2.28) is an important source of Cl during daytime. Photolysis of  $\text{ClNO}_2$  and  $\text{BrCl}$  are also sources of Cl in the environments simulated by the model calculations. Both species are, taken together, of approximately the same importance as the  $\text{HCl} + \text{OH}$  reaction if  $\text{NO}_x$  concentrations are high, or in winter, when both OH and HCl concentrations are lower. Photolysis of  $\text{ClNO}$ ,  $\text{HOCl}$ ,  $\text{ClONO}_2$ , and  $\text{Cl}_2$  are less important. The main source of atomic Br is photolysis of  $\text{Br}_2$ ,  $\text{BrNO}_2$ , and  $\text{BrONO}_2$ . Atomic Br concentrations peak almost two orders of magnitude higher than those of Cl do. The relative importance of each of the species varies with concentration of  $\text{NO}_x$ . Reaction of OH with HBr has been calculated as approximately 3 orders of magni-



tude slower than the photolytic sources. The main loss of atomic Cl and Br from the gas phase takes place through reaction with VOC.

Atomic chlorine takes a part in the catalytic, ozone-destroying chain reaction with interconversion of Cl and ClO (LeBras and Platt, 1995). Cl is oxidised by ozone to ClO that, in turn, may react with several species. Conversion with NO or OH re-circulates Cl directly while reaction with HO<sub>2</sub> forms HOCl that gives Cl on photolysis. In an environment rich in nitrogen oxides and limited in peroxy radicals, the first two reactions dominate and none of them would lead to ozone destruction whereas in a clean environment, limited in oxides of nitrogen, both reaction with OH and with HO<sub>2</sub> lead to ozone depletion. An increase of ozone concentration due to an enhanced peroxy radical formation from the halogen-initiated oxidation of VOC can occur in a polluted environment. The Br - BrO catalytic cycle is governed by reactions corresponding to those of chlorine but in addition, BrO also undergoes fast photolysis, which is a non-ozone destroying channel. The ratio between Br and BrO is substantially higher than the ratio for the corresponding chlorine-species. Paper III investigates the gas-phase chemistry of chlorine species in detail.

The chlorine-containing species are released from the sea-salt aerosol predominantly in the form of HCl. A second important precursor of Cl in the gas-phase is ClNO<sub>2</sub>. Hydrochloric acid is released from the sea-salt particles during daytime while ClNO<sub>2</sub> is produced during nighttime. Small amounts of HOCl are released just after the sunrise due to an intense ClONO<sub>2</sub> formation and subsequent uptake by the liquid particles. This reaction pathway, however, does not lead to dechlorination of particles. Cl<sub>2</sub> is released in very small quantities from the particles when Br<sup>-</sup> is present. When Br<sup>-</sup> is almost completely depleted in the aqueous phase, then equilibria between HOCl, HOBr, Cl<sub>2</sub>, Br<sub>2</sub>, and BrCl are shifted in a way such, that Cl<sub>2</sub> can be released to the gas phase together with BrCl. Bromine is released from the aerosol mainly in the form of Br<sub>2</sub> through the catalytic process described by equations (3.25) and (3.26). Reactive uptake of N<sub>2</sub>O<sub>5</sub> leads to formation of BrNO<sub>2</sub>, which is another, though rather unimportant, gas-phase precursor of atomic bromine. The reactive uptake of BrONO<sub>2</sub>, followed by hydrolysis reaction 3.23 and by equilibria 3.25 and 3.26, leading to Br<sub>2</sub> release, is the most efficient pathway of bromine loss from the sea-salt particles in polluted environments. The way the BrONO<sub>2</sub> reacts in the droplet is not of any great importance since both dihalides are strongly coupled through equilibria in (2.26). BrCl becomes important as a pathway of bromine transport from the aerosol only when Br<sup>-</sup> concentrations are low. When compared to chlorine, bromine is to a large extent recycled through the aerosol particles. When the pollution levels are higher, bromine is almost entirely depleted from the aerosol. However, later on it can be transported back to the aerosol, mainly as HBr, to be released to the gas phase the following morning in the form of Br<sub>2</sub>, and possibly also as BrCl. The sensitivity study described in Paper IV shows the effect of different halogen release pathways in detail.

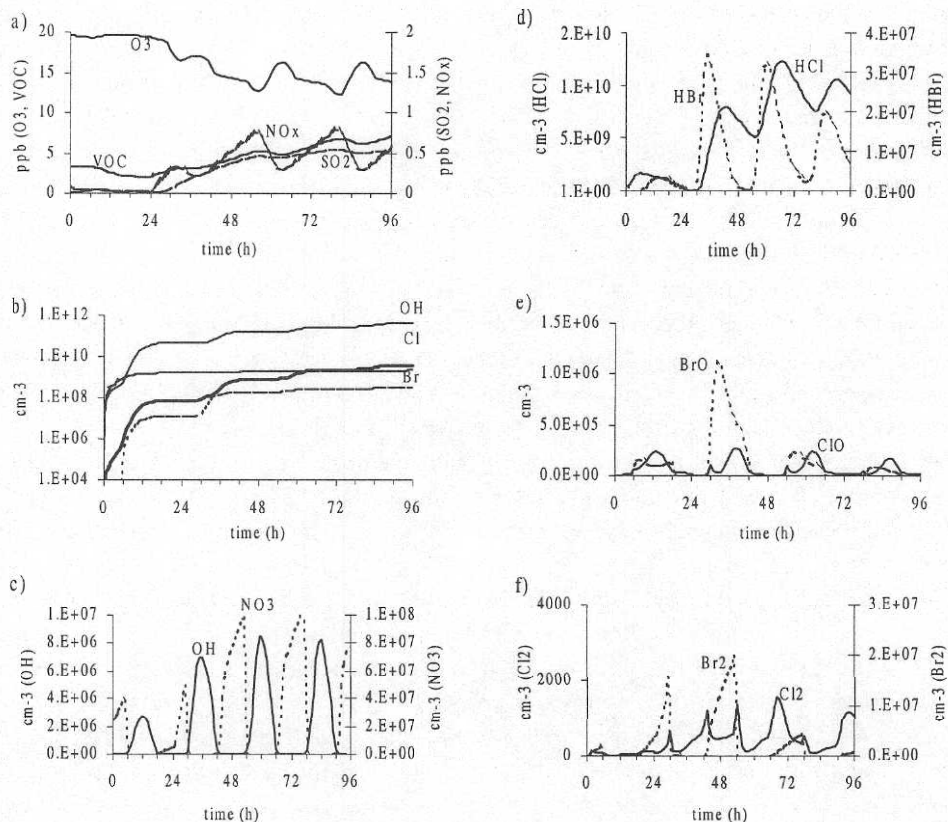
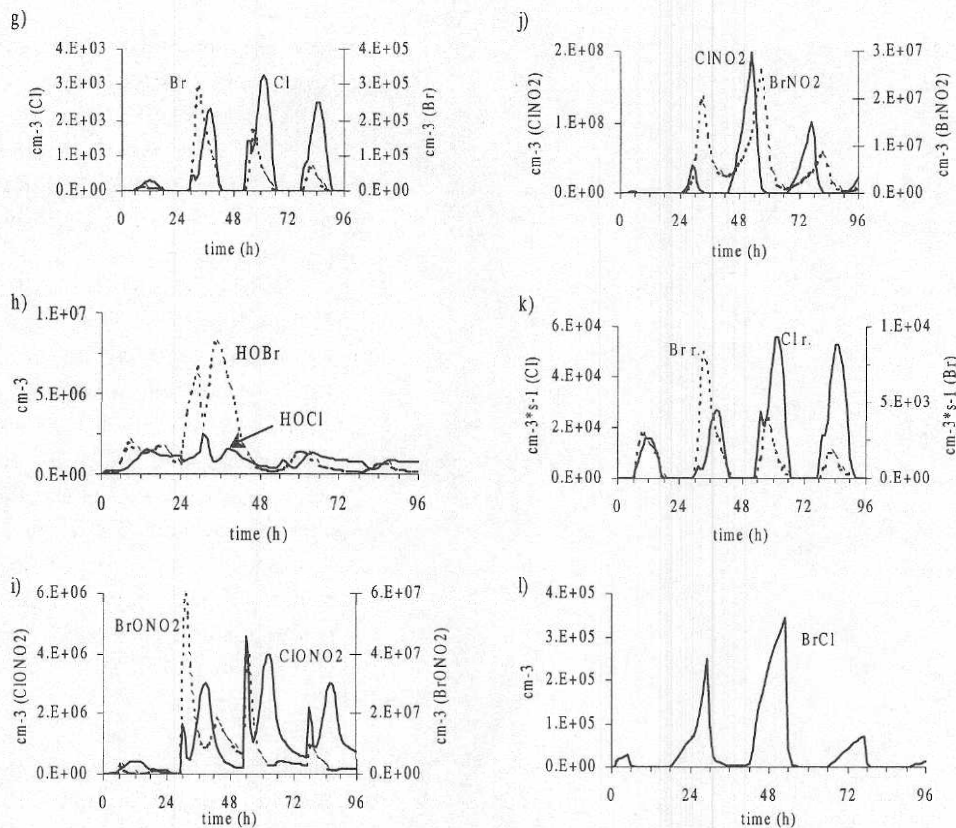


Figure 5 a)-f), For captions, see p. 34.

### 7.3. Effects of sea-salt particles on the troposphere in coastal areas

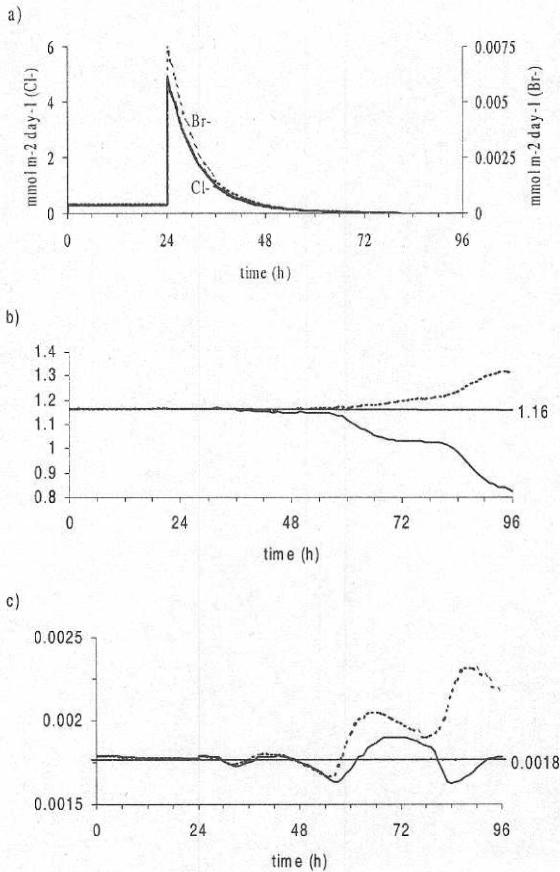
The sea-salt particles affect the tropospheric chemistry at large distances from the coast. Noon concentrations of atomic chlorine of  $3 \times 10^3$  to  $1.3 \times 10^4$  molec.  $cm^{-3}$  were calculated. Maximum simulated concentrations of atomic bromine ranged from  $1 \times 10^5$  to  $1.3 \times 10^6$  molec.  $cm^{-3}$ . The highest values were calculated for air passing a city just at the coast. In this case, the atomic halogen concentrations were increased by almost a factor of two. Concentrations of atomic chlorine and bromine were high also under winter-like conditions. The release of Br from the aqueous phase was more efficient at lower photochemical activity and decreased temperature, mostly due to a more intensive reactive uptake of  $N_2O_5$  and  $BrONO_2$ .

According to the calculations, atomic halogen species did not contribute significantly to



**Figure 5.** Concentration of some gas-phase species in the base-case simulation. a) ozone, non-methane VOC, oxides of nitrogen, and  $\text{SO}_2$ , b) accumulated loss of VOC (including methane) oxidised by OH, ozone, and by atomic Cl and Br, c) OH and  $\text{NO}_3$ , d) atomic Cl and Br, e) HOCl and HOBr, f) HCl and HBr, g) ClO and BrO, h)  $\text{Cl}_2$  and  $\text{Br}_2$ , i)  $\text{ClONO}_2$  and  $\text{BrONO}_2$ , j) loss rate of Cl and Br by reaction with VOC, k)  $\text{ClONO}_2$  and  $\text{BrONO}_2$ , l) BrCl.

the oxidation of VOC under summer conditions. In a clean environment at summer conditions (the base case), approximately 1% of the VOC were oxidised by atomic Cl and around 0.1% by atomic Br. The effect of halogen-initiated oxidation was approximately twice as high in the moderately polluted case as in the base case. During winter conditions, the importance of halogens increased dramatically and in the low temperature, low light intensity case, the chlorine-initiated oxidation of VOC accounted for 10% of the total VOC oxidation and for 29% of the OH-initiated VOC oxidation. The corresponding contribution by the bromine-initiated VOC oxidation was 2 and 4%, respectively. The presence of sea-salt decreased ozone concentrations in a clean coastal environment because of the catalytic atomic halogen – halide monoxide cycle. With increasing concentrations of nitrogen oxides, the ozone destroying potential of the catalytic cycle was reduced. At the same time, the atomic halogen-initiated oxidation of VOC produced peroxy radicals that in further reactions lead to the ozone formation. In the moderately polluted case, the ozone concentrations started to



exceed the concentrations of the corresponding model simulation without the sea-salt particles, after 1.5 day of transport over land. Calculated concentrations of some important species in the base case are shown in Figure 5.

At the coast, the air is filled with sea-salt particles generated by the surf (McKay 1994). The concentration of sea-salt in air rapidly decreases with increasing transport time over land. Figure 6 shows the deposition of sea-salt along the simulated trajectory. Dechlorination of particles finally leads to the formation of HCl, which is also deposited to the surface. Since high

**Figure 6** Deposition of a)  $\text{Br}^-$  and  $\text{Cl}^-$  (in  $\text{mmol m}^{-2} \text{ day}^{-1}$ ) in the base-case simulation, b)  $\text{Cl}^-/\text{Na}^+$  ratio in deposited sea-salt particles (full line) and in dry deposition including both sea-salt deposition and deposition of HCl (dashed line), and c) the same ratios for  $\text{Br}^-$ .

concentrations of HCl are calculated even in air masses transported for 76 hours from the coast, where the sea-salt concentrations are very low, the deposition of  $\text{Cl}^-$  from the gas phase gradually outweighs the  $\text{Cl}^-$  deficit in the deposited particles. The same is true for deposition of  $\text{Br}^-$  in the base case. Deposition of  $\text{Cl}^-$  and  $\text{Br}^-$  related to the  $\text{Na}^+$  deposition from the sea-salt are also shown in Figure 6. Deposition of the sea-salt as a function of the distance from the coast-line has been measured and modelled by Gustafsson (1997) at the Swedish west-coast and by TenHarkel (1997) at the Dutch coast. The sea-salt deposition profile for  $10 \text{ m s}^{-1}$  wind speed published by Gustafsson agrees very well with deposition at the same wind-speed calculated by the present model. The yearly average deposition at the Dutch coast is approximately a factor of 4 lower than that in the model calculations. This value is reasonable since the average wind-speed at the Dutch coast is expected to be less than  $10 \text{ m s}^{-1}$ . Gustafsson and Franzén (1999) measured the  $[\text{Cl}^-]/[\text{Na}^+]$  ratio profile obtained from filters and from pine needle surface deposition after a period with strong winds. While the filter ratios were close to that of seawater (1.16), they measured an excess of  $\text{Cl}^-$  on pine needles



with  $\text{Cl}^-/\text{Na}^+$  ratios between 1.3 and 1.6. In this study, the excess of  $\text{Cl}^-$  was also predicted by the model. After several hours of transport, deposition of gaseous HCl outweighs the Cl deficit in the deposited sea-salt and the  $\text{Cl}^-/\text{Na}^+$  ratio increases above that of the seawater. The winter-half year simulation gave a  $\text{Cl}^-/\text{Na}^+$  ratio 1.35 after one day of transport from the coast.

#### 7.4. Formation of particles from oxidation products of monoterpenes

A detail account of the work referred to in this section is given in Paper V. The EUPHORE reactor in Valencia, Spain, used for investigation of particle formation from the  $\text{NO}_3$ -initiated oxidation products of monoterpenes is shortly described in Paper V, and in detail by Hallqvist *et al.*, (1999). The apparent vapour pressures of oxidation products were estimated from aerosol yields obtained during the experiments with different masses of oxidised terpene by a method described in Paper V. The equilibrium vapour pressures obtained are presented in Table 8. The pressures are too high, considering that nucleation was observed in experiments with conversions of approximately 8 ppb of monoterpenes. With these saturation vapour pressures, the attainable super-saturation (S, cf. Eq. 5.7) would not be much higher than one, while for efficient nucleation, a ratio of 100 or more is needed. This indicates that a small amount of another species with much lower saturation concentration is formed together with the dominant higher volatility product. Assumption of a small yield (1-2%) of a species with very low saturation concentration together with a higher yield of a compound having properties described in Table 8 was the only way of reproducing observations by calculations.

Data from a total particle counter, coupled directly to the reactor was used to estimate nucleation rates. The difference between two adjoining measurements shows the change in number concentration. The actual Nucleation Rate (NR) in the reactor is not directly comparable to the Measured Particle Formation Rate (MPFR) deduced from the particle

**Table 8.** Parameters of the main condensing product used in the model simulations. Gas phase equilibrium concentration  $c_{i0}$  (equivalent to equilibrium vapour pressure  $P_0$ ) and yield  $Y_i$  was estimated from the measured aerosol yields. Molecular weight  $m_w$ , density  $\rho_i$  and surface tension  $\sigma_i$  were set to those of the corresponding low vapour-pressure species.

	$\sigma_i$ ( $\text{N}\cdot\text{m}^{-1}$ )	$\rho_i$ ( $\text{kg}\cdot\text{m}^{-3}$ )	$m_w$ ( $\text{kg}\cdot\text{mol}^{-1}$ )	$c_{i0}$ (ppb)	$P_0$ (Pa)	$Y_i$
$\alpha$ -pinene	2.89E-2	1.08E+3	0.18	0.53	5.37E-5	0.06
$\beta$ -pinene	3.50E-2	1.08E+3	0.15	3.36	3.40E-4	0.50
$\Delta^3$ -carene	3.55E-2	1.00E+3	0.15	6.77	6.86E-4	0.50
limonene:						
primary	3.12E-2	1.08E+3	0.15	2.07	2.10E-4	0.20



**Table 9.** Parameters of the nucleation function (Eq. XI) used in the model simulations. Molecular weight  $m_w$  and density  $\rho_i$  for the nucleating compound were estimated and kept fixed while gas phase equilibrium concentration  $c_{i0}$ , (equivalent to equilibrium vapour pressure  $P_0$ ), yield  $Y_i$ , and surface tension  $\sigma_i$  was tuned to fit simulated nucleation rates to the measured ones.

	$\sigma_i$ ( $N*m^{-1}$ )	$\rho_i$ ( $kg*m^{-3}$ )	$m_w$ $kg*mol^{-1}$	$c_{i0}$ ppt	$P_0$ Pa	$Y_i$
$\alpha$ -pinene	2.89E-2	1.08E+3	0.18	0.20	1.99E-08	0.005
$\beta$ -pinene	3.50E-2	1.08E+3	0.15	0.31	3.18E-08	0.03
$\Delta^3$ -carene	3.52E-2	1.00E+3	0.15	0.20	1.99E-08	0.06
limonene:						
primary	3.12E-2	1.08E+3	0.15	0.18	1.19E-08	0.05
secondary	2.60E-2	1.08E+3	0.15	0.20	1.99E-08	0.68

counter. This is caused by the absent sensitivity to very small particles and by physical processes involving these particles during transport. The model was used as a tool by providing the time of growth from critical size to  $0.012 \mu m$  and the corresponding number loss through coagulation during this time. Table 9 shows the result of a systematic variation of some of the parameters to find a set that reasonably well reproduced the MPFR. The parameter values are result of tuning of the nucleation rate and may not represent real properties of the condensed material. However, it is suggested that they may be used within the concentration range relevant for ambient air as nucleation rate parameterisations.

As may be seen in Table 9, very low vapour pressures of the nucleating substances are required to make the nucleation function work well in the model. The recently identified dicarboxylic acids (Christoffersen *et al.*, 1998, Glasius *et al.*, 1998, Hoffmann *et al.*, 1998) could have such properties, but experimental data are generally not available. Using enthalpies and entropies of sublimation from Davies and Thomas (1960), equilibrium pressures of  $1.3 \times 10^6$ ,  $1.3 \times 10^7$  and  $7.6 \times 10^9$  Pa at 288 K may be calculated for adipic ( $C_6H_{10}O_4$ ), suberic ( $C_8H_{14}O_4$ ) and sebacic ( $C_{10}H_{18}O_4$ ) acid, respectively. The pressures given in Table 9 are of the same order of magnitude as the estimate of the C8 and C10 di-acid vapour pressures, which supports the idea, that di-carboxylic acids in this molecular weight-range may be the nucleating substances.

Significant differences in particle number and mass as well as in size distribution between the four investigated terpenes were noticed. Model simulations, performed for all experiments listed in the Paper confirmed, that the aerosol mass formed depends on yield and vapour pressure of the oxidation products. Since the model used parameters derived from the experimental data (section 3.1), the agreement between calculated and measured aerosol masses was good. Molar yields are presented in Table 8 and 9.  $\alpha$ -pinene was the species giving the lowest aerosol mass, the estimated yield was 7%.  $\beta$ -pinene and  $\Delta^3$ -carene had the greatest yields, giving around 60% of particulate mass under similar conditions. The yield

obtained from limonene was 28% for primary products and 103 % if the aerosol produced by the secondary product was added.

The aerosol number concentration depends on the nucleation rate. Once the nuclei are formed, oxidation products with higher yield and higher equilibrium vapour pressure condense on the nuclei. In this way, the particle number concentration becomes quite independent of the mass concentration that is formed by the main condensing species.

Comparison between the simulated and measured particle number distributions is presented in Paper V. The most common reason for the discrepancies were difficulties with fitting the measured nucleation rates by the nucleation function. Internal variability of experimental data implicated, that there might have been factors not considered in the data evaluation, which affected the experiments.



## 8. Conclusions

Designing atmospheric models is often a difficult and time-consuming work requiring review of many chemical and physical processes. However, once the model is completed, it becomes a powerful tool for gaining an understanding of relations between, and consequences of different atmospheric processes. The reliability of a model is limited by e.g. simplifications involved in description of transport and chemistry, or by the thoroughness of the designer with respect to avoiding nonsense errors. However, the main limitation is the state of knowledge about the processes involved. The model will never become better than its parameters and input data. Sensitivity analysis is the principal way of acquiring an understanding of the complex systems. It can identify processes and parameters, which need to be described with high accuracy, and at the same time find those, which can be simplified or even neglected. Comparison of calculated concentrations with ambient measurements gives valuable information about the model performance. Relating the simulated data directly to the measurements is, however, often difficult due to simplifications employed in the model. One such simplification is the assumption of homogenous concentration within the mixing layer. A series of model simulations, testing the sensitivity of the simulated data to the most important processes in the model and verifying the results against measurements often give information about the performance of a model. Such simulations e.g. showed that a good description of the sources of VOC and NO<sub>x</sub> is of the greatest importance when modelling secondary pollutants.

The NMHC and ozone data from Rörvik, analysed in Paper I, give a rather detailed picture of the secondary pollutant formation and transport in northern Europe throughout the year. The main burden of NMHC transported to the Swedish west coast originates in Western Europe and in the U.K. Transport across the North Sea also brings a major part of the ozone to the south-western Sweden. The distinct seasonal variation of both ozone and NMHC concentrations is related to the change in photochemical activity in troposphere, but some other processes, such as the large-scale mixing, may contribute to the summer to winter change. The statistical description of NMHC and ozone development at Rörvik with respect to seasons and origin of the air masses is often used for initialisation of models or when information about background concentration is needed.

Sea-salt particles affect the tropospheric chemistry at large distances from the coast. Noon concentrations of  $3 \times 10^3 - 1.3 \times 10^4$  molec. cm<sup>-3</sup> of atomic chlorine and  $1 \times 10^5 - 1.3 \times 10^6$  molec. cm<sup>-3</sup> of atomic bromine were calculated. Atomic halogen species, as calculated for summer conditions, did not contribute significantly to the VOC oxidation. However, during winter conditions the importance increased dramatically and in the low temperature, low light intensity case, the chlorine-initiated oxidation of VOC accounted for 29% of the OH-initiated VOC oxidation.

The sea-salt has an ozone reducing effect in clean air due to the catalytic atomic halogen – halogen monoxide cycle. With increasing concentrations of nitrogen oxides, the ozone destroying potential of the catalytic cycle is reduced at the same time as the atomic halogen-initiated oxidation of VOC produces peroxy radicals that in further reactions lead to ozone formation. In the model calculations presented in Paper IV, the ozone concentrations were altered by a few ppb at the most.

The CCDSSP model describes well deposition of sea-salt when compared with measurements. With increasing time of transport from the coast, the sea-salt deposition becomes less important at the same time, as deposition of HCl keeps almost constant. This means, that the Cl<sup>-</sup> deficiency in the deposited sea-salt is fully compensated for, and an excess of Cl<sup>-</sup> is found because of HCl deposition. The excess Cl<sup>-</sup> is coupled with acidity which is often not accounted for in deposition measurements.

During the nitrate radical oxidation of  $\beta$ -pinene,  $\Delta^3$ -carene and limonene, and during oxidation of monoterpenes in general, particulate matter is formed. In this way reactive species are removed from the gas phase, thereby excluding this fraction of the organic matter from participation e.g. in the tropospheric ozone formation. At the same time formation of new particles has a potential to affect the energy balance of the Earth. The calculations presented in Paper V indicate that some of the terpene oxidation products have a large particle formation potential even in an environment with high background particle concentration. The nucleation rate, as it is described in the model, is critically dependent on several parameters and it is not possible to decide which, in practice, is the more important. It is nevertheless clear that the equilibrium vapour pressure of the nucleating substance has a decisive influence. The nucleating substance(s) must have a vapour pressure in the  $10^{-7}$  -  $10^{-8}$  Pa region in order to produce the necessary super-saturation to induce nucleation. However, the yield of this product need not be high if the vapour pressure is low enough. Di-carboxylic acids are candidate substances, as was recently observed (Christoffersen *et al.*, 1998, Glasius *et al.*, 1998, Hoffmann *et al.*, 1998). The parameterised nucleation description given in paper V could be used in detailed atmospheric models involving the terpenes in question.



## Acknowledgements

The financial support from Swedish Environmental Protection Agency, Swedish Environmental Research Institute (IVL), Carl Tryggers Stiftelse and the EU Environment and Climate BIOVOC project ENV4CT95 0059 is gratefully acknowledged.

Special thanks are to my supervisor, professor Evert Ljungström for his inexhaustible support, encouragement, scientific advice and practical help during the years.

Professor Oliver Lindquist is acknowledged for providing me with the opportunity to perform research at the department of Inorganic Chemistry

During the time spent at the department of Inorganic Chemistry of Göteborg University, I met scientists, colleagues, and friends who encouraged me in my work with their help and interest. I wish to thank to all of them and namely to Dr Sarka Langer, Dr. Mattias Hallquist, Albert Chan, Dr. Ingvar Wängberg, Dr. Rune Karlsson, Jun Noda, Maria Ullerstam, Dongmei Zhao for their help and for creating a pleasant atmosphere to work at.

Dr. Vratislav Langer, Dr. Anders Snis and Roger Sagdahl are acknowledged for support and advise with computers.

Part of this work was done at IVL, Göteborg. Dr. Anne Lindskog, Dr. Yvonne Andersson-Sköld, Carin Pleijel and professor Peringe Grennfeldt are acknowledged for introducing me to the field of atmospheric chemistry and modelling. Thanks to Anne for exciting discussions about the mysteries of VOC and to Jacques Mowrer, who did the VOC measurements.

I want to give a very special thanks to Filip, for his encouragement and confidence in my abilities. Thank you for your love and support, Filip, Petr and Jakub.



## References

- AEA Technology (1994) *FACSIMILE, Process & chemical reaction modeller manual*, AEATEchnology, Harwell, Didcot, Oxfordshire, U.K.
- Andreae, M.O. and Crutzen, P.J. (1997) Atmospheric aerosols: Biogeochemical sources and role in atmospheric chemistry. *Science*, **276**, 1052-1058.
- Arnts, R.R. and Meeks, S. (1981) Biogenic hydrocarbon contribution to the ambient air of selected areas. *Atmos. Environ.* **15**, 1643-1653.
- Atkinson, R. (1997) Gas-phase tropospheric chemistry of volatile organic compounds 1. Alkanes and alkenes. *J. Phys. Chem. Ref. Data*, **26**, 215-290.
- Atkinson, R., Baulch, D. L., Cox, R. A., Hampson Jr., R. F., Kerr, J. A., and Troe, J. (1997) Evaluated kinetics, photochemical and heterogeneous data for atmospheric chemistry, Supplement V, *J. Phys. Chem. Ref. Data*, **26**, 521-1011.
- Austin, J. F., Follows, M. J. (1991) The Ozone Record at Payerne: an Assessment of the Cross-Tropopause Flux. *Atmos. Environ.*, **25**, No. 9, pp. 1873-1880.
- Barrie, L. A., Bottenheim, J. W., Schnell, R. C., Crutzen, P. J., and Rasmussen, R. A. (1988) Ozone destruction and photochemical reactions at polar sunrise in the lower Arctic atmosphere. *Nature*, **334**, 138-141.
- Beckwith, R. C., Wang, T. X., and Margerum, D. W. (1996) Equilibrium and kinetics of bromine hydrolysis. *Inorg. Chem.*, **35**, 995-1000.
- Behnke, W., George, C., Scheer, V., and Zetzsch, C. (1997) Production and decay of ClNO<sub>2</sub>, from the reaction of gaseous N<sub>2</sub>O<sub>5</sub> with NaCl solution: Bulk and aerosol experiments. *J. Geophys. Res.* **102**, 3795-3804.
- Behnke, W., Sheer, V., and Zetzsch, C. (1994) Production of BrNO<sub>2</sub>, Br<sub>2</sub> and ClNO<sub>2</sub> from the reaction between sea spray aerosol and N<sub>2</sub>O<sub>5</sub>. *J. Aerosol Sci.* **25**, S277-S278.
- Behnke, W., and Zetzsch, C. (1989) Heterogeneous formation of chlorine atoms from various aerosols in the presence of O<sub>3</sub> and HCl. *J. Aerosol Sci.*, **20**, 1167-1170.
- Blanchard, D. C., and Woodcock, A. H. (1980) The production, concentration, and vertical distribution of the sea-salt aerosol. *Annals New York Academy of Sciences* **338**, 330-347.
- Bojkov, R.D. (1986) Surface ozone during the second half of the nineteenth century, *J. Of Climate and Appl. Meteor.*, **25**, 343-352.
- Christoffersen, T.S., Hjorth, J., Horie, O., Jensen, N.R., Kotzias, D., Molander, L.L., Neeb, P., Ruppert, L., Winterhalter, R., Virkkula, A., Wirtz, K. and Larsen, B.R. (1998) Cis-pinic acid, a possible precursor for organic aerosol formation from ozonolysis of  $\alpha$ -pinene. *Atmos. Environ.*, **32**, 1657-1661.
- Cohen, M. D., Flagan, R. C., and Sienfeld, J. H. (1987) Studies of concentrated electrolyte solutions using the electrodynamic balance. 3. Solute nucleation. *J. Phys. Chem.*, **91**, 4583-4590.
- Crump, J.G. and Seinfeld, J.H. (1981) Turbulent deposition and gravitational sedimentation of an aerosol in a vessel of arbitrary shape. *J. Aerosol Sci.*, **12**, 405-415.
- Crutzen P.J., and Gidel, L.T. (1983) A two-dimensional photochemical model of the atmosphere. 2: The tropospheric budgets of the anthropogenic chlorocarbons, CO, CH<sub>4</sub>, CH<sub>3</sub>Cl, and the effect of various NO<sub>x</sub> sources on tropospheric ozone, *J. Geophys. Res.*, **88**, 6641-6652.
- Curtis, A.R., Sweetenham, W.P. (1987) *FACSIMILE/CHEKMAT User's Manual*, UK Atomic Energy Authority, Harwell Laboratory, Oxfordshire, AERE R 12805.
- Davidson, C.I., Wu, Y.L. (1990) Dry Deposition of Particles and Vapours, in *Acidic Precipitation*, Vol. 3, Sources, Deposition and Canopy Interactions, ed. Lindberg et al., Springer-Verlag.
- Davies, M. and Thomas, G.H. (1960) The lattice energies, infra-red spectra, and possible cyclization of some dicarboxylic acids. *Trans. Faraday Soc.*, **56**, 185-192.
- Demerjian, K. L., Schere, K. L., and Peterson, J. T. (1980). Theoretical estimates of actinic (spherically integrated) flux and photolytic rate constants of atmospheric species in the lower troposphere. *Adv. Environ. Sci. Technol.*, **10**, 369-460.

## References

- DeMore, W. B., Sander, S. P. Golden, D. M., Hampson, R. F., Kurylo, M. J., Howard, C.J., Ravishankara, A. R., Kolb, C. E., and Molina, M. J. (1997) *Chemical Kinetics and photochemical data for use in stratospheric modelling.*, Eval. 12., Jet Propul. Lab., Pasadena, California.
- Finlayson-Pitts, B. J., and Pitts Jr., J. N. (2000) *Chemistry of the Upper and Lower Atmosphere*. Academic Press, A Harcourt Science and Technology Company, San Diego, California.
- Finlayson-Pitts, B. J. (1993) Chlorine atoms as a potential tropospheric oxidant in the marine boundary layer. *Res. on Chem. Intermed.*, **19**, 235-249.
- Finlayson-Pitts, B. J., Ezell, M. J., and Pitts Jr., J. N. (1989) Formation of chemically active chlorine compounds by reactions of atmospheric NaCl particles with gaseous N<sub>2</sub>O<sub>5</sub> and ClONO<sub>2</sub>. *Nature*, **337**, 241-244.
- Gery, M. W., Whitten, G. Z., Killus, J. P., and Dodge, M. C. (1989) A photochemical mechanism for urban and regional scale computer modelling. *J. Geophys. Res.*, **94**, 12925-12956.
- Glasius, M., DiBella, D., Lahaniati, M., Calogirou, A., Jensen, N.R., Hjorth, J., Kotzias, D. and Larsen, B.R. (1998) Identification of carboxylic acids in aerosol produced by gas phase oxidation of monoterpenes. *Environ. Sci. Pollut. Res.*, **5**, 146.
- Graedel, T. E., and Keene, W. C. (1995) Tropospheric budget of reactive chlorine. *Global Biogeochemical Cycles*, **9**, 47-77.
- Guenther, A., Hewitt, C.H., Erickson, D., Fall, R., Geron, C., Graedel, T., Harley, P., Klinger, L., Lerdau, M., McKay, W.A., Pierce, T., Scholes, B., Steinbrecher, R., Tallamraju, R., Taylor, J. and Zimmerman, P. (1995) A global model of natural volatile organic compound emissions. *J. Geophys. Res.*, **100**, 8873-8892.
- Gustafsson, M. E. R. (1997) Raised levels of marine aerosol deposition owing to increased storm frequency; a cause of forest decline in southern Sweden? *Agricultural and Forest Meteorol.*, **84**, 169-177.
- Gustafsson, M. E. R., and Franzén, L.G. (1999) Inland transport of marine aerosols in southern Sweden. *Atmos. Env.*, **34**, 313-325.
- Hallquist, M., Wängberg, I., Ljungström, E., Barnes, I. and Becker, K.H. (1999) Aerosol and product yields from NO<sub>3</sub> radical-initiated oxidation of selected monoterpenes. *Environ. Sci. Technol.*, **33**, 553-559.
- Heintz F., Platt U., Flentje H., and Dubois R. . 1996. Long-term observation of nitrate radicals at the tor station, Kap Arkona (Rugen). *J. Geophys. Res.*, **101**, 22891-22910.
- Heisler, S.I. and Friedlander, S.K. (1977) Gas-to-particle conversion in photochemical smog: aerosol growth laws and mechanisms for organics. *Atmos. Environ.*, **11**, 157 - 168.
- Hesstvedt E., Hov Ø., Isaksen, I. (1978) Quasi-Steady-State Approximations in Air Pollution Modelling: Comparison of Two Numerical Schemes for Oxidant Prediction. *Int. J. Chem. Kin.*, **10**, 971-994.
- Hoffmann, T., Bandur, R., Marggraf, U. and Linscheid, M. (1998) Molecular composition of organic aerosols formed in the alpha-pinene/O<sub>3</sub> reaction; Implications for new particle formation processes. *J. Geophys. Res.*, **103**, 25569-25578.
- Holland F., Aschmutat U., Hessling M., Hofzumahaus A., and Ehhalt D.H. (1998) Highly time resolved measurements of OH during POPCORN using laser-induced fluorescence spectroscopy. *J. Atm. Chem.*, **31**, 205-25.
- Hov, Ø., Schmidbauer, N. (1992) Atmospheric concentrations of nonmethane Hydrocarbons at a North European Coastal Site. *J. Atm. Chem.*, **14**, 515-526.
- Huie, R.E. and Netta, P. (1987) Rate constants for some oxidations of S(IV) by radicals in aqueous solutions. *Atmos. Environ.*, **21**, 1743-1747.
- Jacob, D. J. (1986) Chemistry of OH in remote clouds and its role in the production of formic acid and peroxymonosulfate, *J. Geophys. Res.*, **91**, 9807-9826.
- Jayson, G. G., Parsons, B. J., and Swallow, A. J. (1973) Some simple, highly reactive, inorganic chlorine derivatives in aqueous solution. Their formation using pulses of radiation and their role in the mechanism of the fricke dosimeter., *J. Chem. Soc. Farraday Transactions*, **69**, 1597-1607.



## References

- Jobson, B. T., Niki H., Yokouchi Y., Bottenheim J., Hopper F., and Leitch R. (1994) Measurements of C-2-C-6 hydrocarbons during the Polar Sunrise 1992 Experiment - evidence for Cl atom and Br atom chemistry. *J. Geophys. Res.*, **99**, 25355-25368.
- Junge, C. E. (1957) Chemical analysis of aerosol particles and gas tracers on the island of Hawaii. *Tellus*, **9**, 528-537.
- Keene, W. C., Sander, R., Pszenny, A. A. P., Vogt, R., Crutzen, P. J., and Galloway, J. N. (1998) Aerosol pH in the marine boundary layer: A review and model evaluation. *J. Aeros. Sci.*, **29**, 339-356.
- Keene, W. C., Pszenny, A. P., Jacob, D. J., Duce, R. A., Galloway, J. N., Schultz-Tokos, J. J., Sievering, H., and Boatman, J. F. (1990) The geochemical cycling of reactive chlorine through the marine troposphere. *Global Biogeochemical Cycles*, **4**, 407-430.
- Kim, Y. P., Sievering, H., and Boatman, J. (1990) Volume and surface area size distribution, water mass and model fitting of GCE/CASE/WATOX marine aerosols. *Global Biogeochemical Cycles*, **4**, 165-177.
- Kläning, U.K., Wolf, T. (1985) Laser flash photolysis of HClO ClO<sup>-</sup>, HBrO, and BrO<sup>-</sup> in aqueous solution, Reactions of Cl<sup>-</sup> and Br<sup>-</sup> atoms. *Ber. Bunsenges Phys. Chem.*, **89**, 243-245.
- Kumar, K., and Margerum, D. W. (1987) Kinetics and mechanism of general-acid-assisted oxidation of bromide by hypochlorite and hypochlorous acid. *Inorg. Chem.*, **26**, 2706-2711.
- Lamb, B., Guenther, A., Gay, D. and Westberg, H. (1987) A national inventory of biogenic hydrocarbon emissions. *Atmos. Environ.*, **21**, 1695-1705.
- Laux, J. M., Hemminger, J. C., and FinlaysonPitts, B. J. (1994) X-Ray Photoelectron Spectroscopic Studies of the Heterogeneous Reaction of Gaseous Nitric-Acid with Sodium-Chloride - Kinetics and Contribution to the Chemistry of the Marine Troposphere. *Geophys. Res. Lett.*, **21**, 1623-1626.
- LeBras, G., and Platt, U. (1995) A possible mechanism for combined chlorine and bromine catalyzed destruction of tropospheric ozone in the arctic. *Geophys. Res. Lett.*, **22**, 599-602.
- Lee, F. S. C., and Rowland, F. S. (1977) Thermal chlorine-38 reactions with propene. *J. Phys. Chem.*, **81**, 1222-1229.
- Lelieveld, J., and Crutzen, P. J. (1991) The role of clouds in tropospheric photochemistry, *J. Atmos. Chem.*, **12**, 229-267.
- Lovett, R. F. (1978) Quantitative Measurements of Airborne Sea-Salt in the North Atlantic. *Tellus*, **30**, 358-364.
- Madronich, S. (1987) Photodissociation in the atmosphere. 1. Actinic flux and the effects of ground reflections and clouds. *J. Geophys. Res.*, **92**, 9740-9752.
- McKay, W. A., Garland, J. A., Livesley, D., Halliwell, C. M., and Walker, M. I. (1994) The characteristics of the shore-line sea spray aerosol and the landward transfer of radionuclides discharged to coastal sea-water. *Atmos. Env.*, **28**, 3299-3309.
- Millero, F. J., and Sohn, M. L. (1991) *Chemical Oceanography*, CRC Press, Boca Raton, Florida.
- Moldanová J. (1994) *Oxidant Formation in the Troposphere. A Modelling Study of the Role of Photochemistry, Transport and Source Strength of Individual Hydrocarbons*. report OOK94:1, Göteborg, Sweden.
- Monson, R., Jaeger, C., Adams, W., Driggers, E., Silver, G. and Fall, R. (1992) Relationships among isoprene emission rate, photosynthesis, and isoprene synthase activity as influenced by temperature. *Plant Physiol.*, **92**, 1175-1180.
- Mount G.H., Brault J.W., Johnston P.V., Marovich E., Jakoubek R.O., Volpe C.J., Harder J., and Olson J. (1997) Measurement of tropospheric OH by long-path laser absorption at Fritz Peak Observatory, Colorado, during the OH Photochemistry Experiment, Fall 1993. *J. Geophys. Res.*, **102**, 6393-6413.
- Mowrer, J. and Lindskog, A. (1991). Automatic unattended sampling and analysis of background levels of C2-C5 hydrocarbons. *Atmo. Environ.*, **25**, 1971-1979.
- Mozurkewich, M. (1995) Mechanisms for the release of halogens from sea-salt particles by free radical reactions. *J. Geophys. Res.*, **100**, 14199-14207.
- Neta, P., Huie, R. E., and Ross, A. B. (1990) Rate constants for reactions of inorganic radicals in aqueous solution. *J. Phys. Chem. Ref. Data*, **19**, 1027-1260.



## References

- Netter, J., Wasserman, W., Kutner, M.H., (1990), *Applied Linear Statistical Models, Regression, Analysis of Variance and Experimental Designs*. IRWIN, Homewood, Boston.
- Niki, H., Maker, P. D., Savage, C. M., and Breitenbach, L. P. (1980) An FTIR study of the Cl atom-initiated oxidation of  $\text{CH}_2\text{Cl}_2$  and  $\text{CH}_3\text{Cl}$ . *Int. J. Chem. Kinetics*, **12**, 1001-1012.
- Niki, H., Maker, P. D., Savage, C. M., and Hurley, M. D. (1987) Fourier transform infrared study of the kinetics and mechanisms for the Cl-atom- and OH-radical- initiated oxidatin of glycolaldehyde. *J. Phys. Chem.* **91**, 2174-2178.
- Noda, J., Hallquist, M., Langer, S., Ljungström, E. (2000) Products from the gas-phase reaction of some unsaturated alcohols with nitrate radicals, *Phys. Chem. Chem. Phys.*, in print.
- Oxtoby, D.W. (1992) Homogeneous nucleation - theory and experiment. *J. Phys.-cond. Matter*, **4**, 7627-7650.
- Perner, D., Platt, U., Trainer, M., Hübler, G., Drummond, J., Junkermann, W., Rudolph, J., Shubert, B., Voltz, A. and Ehhalt, D.H. (1987) Measurements of Tropospheric OH Concentrations: A Comparison of Field Data. *J. Atmos. Chem.*, **9**, 185-216.
- Pitzer, K. S., *Activity Coefficients in Electrolyte Solutions*, CRC Press, Boca Raton, Florida, 1991.
- Platt, U., Rateike, M., Junkermann, W. Rudolph, J., Ehhalt D.H. (1988) New Tropospheric OH Measurements. *J. Geophys. Res.*, **93**, 5159 - 5166.
- Plummer, L. N., Parkhurst D. L., Fleming G. W., and Dunkle S. A. (1988) *A Computer Program Incorporating Pitzer's Equations for Calculatinon of Geochemical Reactions in Brines*, U.S. Geological Surway, Water-Resources Investigations Report 88-4153, Reston, Virginia.
- Rood, M. J., Shaw, M. A., Larson, T. V., and Covert, D. S. (1989) Ubiquitous nature of ambient metastable aerosol. *Nature*, **337**, 537-539.
- Ruggaber, A., Dlugi, R., Bott, A., Forkel, R., Herrmann, H., and Jacobi, H. W. (1997)-Modelling of radiation quantities and photolysis frequencies in the aqueous phase in the troposphere. *Atmos. Env.*, **31**, 3135-31348.
- Sander, R., and Crutzen. P.J. (1996) Model study indicating halogen activation and ozone destruction in polluted air masses transported to the sea. *J. Geophys. Res.*, **101**, 9121-9138.
- Schwartz, S. E. (1986) Mass-transport considerations pertinent to aqueous phase reactions of gases in liquid-water clouds. *NATO-ASI Series G-Chemistry of Multiphase Atmospheric Systems G6*: 415-471.
- Seinfeld, J. H., and Pandis, S.N. (1998) *Atmospheric Chemistry and Physics. From Air Pollution to Climate Change*, John Wiley & Sons, New York.
- Seinfeld, J.H. (1986) *Atmospheric Chemistry and Physics of Air Pollution*. John Wiley, New York.
- Simpson, D., Winiwarter, W., Borjesson, G., Cinderby, S., Ferreiro, A., Guenther, A., Hewitt, C.N., Janson, R., Khalil, M.A.K., Owen, S., Pierce, T.E., Puxbaum, H., Shearer, M., Skiba, U., Steinbrecher, R., Tarrason, L. and Oquist, M.G. (1999) Inventorying emissions from nature in Europe. *J. Geophys. Res.*, **104**, 8113-8152.
- Stahelin J., and Schmid W. (1991) Trend analysis of tropospheric ozone concentrations utilizing the 20-year data set of ozone balloon soundings over payerne (Switzerland). *J. Geophys. Res.*, **25**, 1739-1749.
- Tang, I. N. (1997) Thermodynamic and optical properties of mixed-salt aerosols of atmospheric importance. *J. Geophys. Res.*, **102**: 1883-1893.
- Tang, I. N., and Munkelwitz, R. (1993) Composition and temperature dependence of the deliquescence properties of hygroscopic aerosols. *Atmos. Environ.*, **27**, 467-473.
- TenHarkel, M. J. (1997) The effects of particle-size distribution and chloride depletion of sea-salt aerosols on estimating atmospheric deposition at a coastal site. *Atmos. Environ.*, **31**, 417-427.
- Vogt, R., Crutzen, P. J., and Sander, R. (1996) A mechanism for halogen release from sea-salt aerosol in the remote marine boundary layer. *Nature*, **383**, 327-330.
- Wang, S.C., Flagan, R.C. and Seinfeld, J.H. (1992) Aerosol formation and growth in atmospheric organic/NO<sub>x</sub> systems - II. Aerosol dynamics. *Atmos. Environ.*, **26**, 421-434.

### References

- Wang, T. X., Kelley, M. D., Cooper, J. N., Beckwith, R. C., and Margerum, D. W. (1994) Equilibrium, kinetic, and UV-spectral characteristics of aqueous bromine chloride, bromine, and chlorine species. *Inorg. Chem.*, **33**, 5872-5878.
- Wang, T. X., and Margerum, D. W. (1994) Kinetics of Reversible Chlorine Hydrolysis - Temperature-Dependence and General Acid Base-Assisted Mechanisms. *Inorg. Chem.*, **33**, 1050-1055.
- Woodcock, A. H. (1953) Salt nuclei in marine air as a function of altitude and wind force. *J. Meteorol.*, **10**, 362-371.



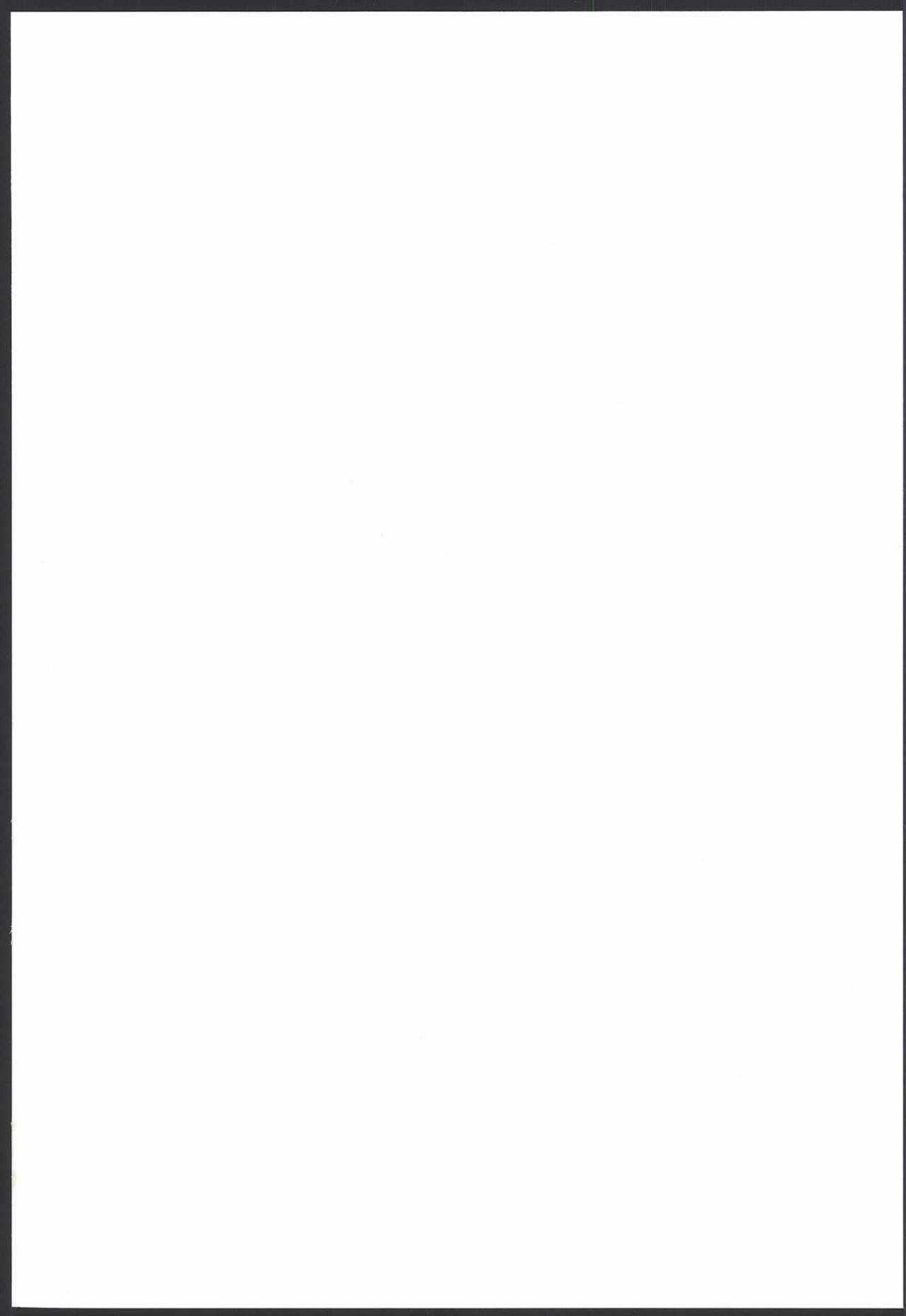
På grund av upphovsrättsliga skäl kan vissa ingående delarbeten ej publiceras här.  
För en fullständig lista av ingående delarbeten, se avhandlingens början.

Due to copyright law limitations, certain papers may not be published here.  
For a complete list of papers, see the beginning of the dissertation.











GÖTEBORG  
UNIVERSITY

Faculty of Science

ISBN 91-628-4220-X